# Zinc Influence on the Formation and Properties of Pt/Mg(Zn)AlO x Catalysts Synthesized From Layered Hydroxides

Belskaya, O. B.; Stepanova, L. N.; Gulyaeva, T. I.; Erenburg, S. B.; Trubina, S. V.; Kvashnina, K.; Nizovskii, A. I.; Kalinkin, A. V.; Zaikovskii, V. I.; Bukhtiyarov, V. I.; Likholobov, V. A.;

Originally published:

June 2016

**Journal of Catalysis 341(2016), 13-23**

DOI: https://doi.org/10.1016/j.jcat.2016.06.006

Perma-Link to Publication Repository of HZDR:

https://www.hzdr.de/publications/Publ-23543


# Zinc Influence on the Formation and Properties of Pt/Mg(Zn)AlO $_x$ Catalysts Synthesized From Layered Hydroxides

O.B. Belskaya, L.N. Stepanova, T.I. Gulyaeva, S.B. Erenburg, S.V. Trubina, K. Kvashnina, A.I. Nizovskii, A.V. Kalinkin, V.I. Zaikovskii, V.I. Bukhtiyarov, V.A. Likholobov

PII: S0021-9517(16)30086-0
DOI: http://dx.doi.org/10.1016/j.jcat.2016.06.006
Reference: YJCAT 12124

To appear in: *Journal of Catalysis*

Received Date: 2 March 2016
Revised Date: 2 June 2016
Accepted Date: 6 June 2016

Please cite this article as: O.B. Belskaya, L.N. Stepanova, T.I. Gulyaeva, S.B. Erenburg, S.V. Trubina, K. Kvashnina, A.I. Nizovskii, A.V. Kalinkin, V.I. Zaikovskii, V.I. Bukhtiyarov, V.A. Likholobov, Zinc Influence on the Formation and Properties of Pt/Mg(Zn)AlO $_x$ Catalysts Synthesized From Layered Hydroxides, *Journal of Catalysis* (2016), doi: http://dx.doi.org/10.1016/j.jcat.2016.06.006

# Zinc Influence on the Formation and Properties of Pt/Mg(Zn)AlO$_x$ Catalysts Synthesized From Layered Hydroxides

O.B. Belskaya[a,b*], L.N. Stepanova[a], T.I. Gulyaeva[a], S.B. Erenburg[c,d], S.V. Trubina[c], K. Kvashnina[e], A.I. Nizovskii[f,b], A.V. Kalinkin[f], V.I. Zaikovskii[f,g], V.I. Bukhtiyarov[f,g], V.A. Likholobov[a,b]

[a] *Institute of Hydrocarbons Processing SB RAS, Neftezavodskaya st., 54, 644040 Omsk, Russia*

[b] *Omsk State Technical University, Mira ave., 11, 644050 Omsk, Russia*

[c] *Nikolaev Institute of Inorganic Chemistry SB RAS, Acad. Lavrentieva ave., 3, 630090 Novosibirsk, Russia*

[d] *Budker Institute of Nuclear Physics SB RAS, Acad. Lavrentieva ave., 11, 630090 Novosibirsk, Russia*

[e] *ESRF-The European Synchrotron, CS40220, 38043 Grenoble Cedex 9, France*

[f] *Boreskov Institute of Catalysis SB RAS, Acad. Lavrentieva ave., 5, 630090 Novosibirsk, Russia*

[g] *Novosibirsk State University, Pirogova str. 2, 630090 Novosibirsk, Russia*

**Corresponding author:** Olga B. Belskaya

Present address: Institute of Hydrocarbons Processing, Siberian Branch of the Russian Academy of Sciences, Neftezavodskaya st., 54, 644040 Omsk, Russia

E-mail: obelska@ihcp.ru

Tel.: +7 (3812) 670 474, fax: +7 (3812) 646 156

**Abstract:**

Layered double hydroxides (LDH) containing $Al^{3+}$, $Mg^{2+}$ and $Zn^{2+}$ cations with the ratios of Zn/(Mg+Zn) = 0, 0.05, 0.1, 0.2, 0.5, 0.7, and 1.0 were synthesized. The effect of zinc content on the phase composition of LDH and on the structural parameters, textural characteristics and acid-base properties of the corresponding mixed oxides were studied. This type of supports was used to obtain the non-acid platinum Pt/Mg(Zn)$AlO_x$ catalysts. The formation of supported platinum particles, their composition, dispersion and electronic state were examined by means of TPR, TEM, XPS, and EXAFS. The possibility to obtain the bimetallic PtZn particles, whose structure and strength of interaction with the support depend on the zinc content of the support, was demonstrated. It was found that the presence of zinc atoms in the platinum environment decreases the particle size of active metal and stabilizes platinum in the active metallic state ensuring a high activity of the catalyst in dehydrogenation of propane with the selectivity for propylene above 99%.

**Keywords:** zinc containing layered double hydroxides, platinum catalysts, propane dehydrogenation, XPS, EXAFS

## 1. Introduction

Layered double hydroxides (LDH) with the general formula $[M(II)_{1-x}M(III)_x(OH)_2][A^{n-}]_{x/n}\ mH_2O$, where *M* is a metal and *A* is an anion, are widely employed in various fields [1-6]. The catalytic application of these materials is related to the synthesis of multicomponent catalysts for aldol condensation, alkylation, polymerization, hydrogenation, steam reforming and other reactions [7-10]. The main advantages of LDH as catalyst precursors list the possibility to use various cationic pairs in the formation of a layered structure and hence the synthesis of materials with different controllable properties; the distribution of cations in the LDH structure at the atomic level, which prevents their significant segregation during further treatments; the formation of mixed oxides with a developed surface area upon decomposition of LDH. The application of mixed oxides produced by thermal treatment of magnesium-aluminum LDH as non-acid supports for platinum catalysts ensures the high stability of the catalysts under the coking conditions and during the redox treatment [11, 12]. Thus, one of the promising applications of such catalysts is the high-temperature dehydrogenation of alkanes [13 - 21]. Particular attention is drawn to the supports containing LDH, where aluminum or magnesium cations are partially substituted by other elements that are able not only to affect the characteristics of support (textural parameters and acid-base properties) but also to modify the properties of platinum [18-21].

Modification of the catalytic behavior of a noble metal by adding the second inactive metal that can form an alloy or intermetallic compound is a topical field in heterogeneous catalysis [22-28]. The brightest example is the platinum-tin system supported on alumina. This composite has been widely used in gasoline reforming and dehydrogenation of alkanes, demonstrating higher activity and stability as compared with monometallic platinum catalyst [22-28]. The mechanism of the promoting action of tin was studied in detail. Tin and platinum are supposed to form

bimetallic alloys of different composition, which ensure the dissociative adsorption of alkanes and diminish the adsorption of alkenes as the target products. Platinum-tin catalysts can be synthesized also with $SiO_2$, zeolites [29, 30] and stoichiometric spinels [34, 36] as the supports; such catalysts are employed in dehydrogenation of light alkanes, oxidation of CO, and selective hydrogenation of the carbonyl group in unsaturated aldehydes [34-39]. Platinum-tin composites supported on mixed oxides made from magnesium-aluminum LDH are also known. In this case, the step of anchoring the active component, which excludes structural transformations of the oxide support, is quite complicated. It consists in the deposition of either a colloidal suspension of bimetallic PtSn particles or acetylacetonate complexes of platinum and tetra n-butyl tin in organic solvents in the absence of air [16-17]. A more promising method of adding a modifier is its introduction in the oxide support precursor, LDH. Thus, in some works [18-21], the properties of platinum were modified by introducing indium and gallium cations into MgAl-LDH during coprecipitation of hydroxides.

The purpose of the present work was to synthesize the LDH containing aluminum, magnesium and zinc cations upon variation of the zinc fraction in the composition of bivalent components, and to elucidate the effect of zinc content on the properties of oxide supports and supported platinum. Dehydrogenation of propane served as a model reaction for estimating the effect of the composition of support on the dehydrogenating activity of platinum.

The effect of the features of a bivalent metal on the structural and textural characteristics of LDH and the corresponding mixed oxides was studied in our earlier work [40]. It was shown that the structure and properties of zinc-containing LDH are close to those of magnesium-aluminum system, and these LDH can form the oxide phase with a developed surface area. The use of zinc for modification of platinum properties is well known [22, 41-43]. The platinum-zinc system resembles the platinum-tin one. Platinum and zinc also can form alloys of different stoichiometry (for example, PtZn and $Pt_3Zn$), which differ from monometallic platinum catalysts in the

catalytic properties. In addition, zinc oxide is the *n*-type semiconductor, and its strong interaction with platinum is quite expectable. Therefore, platinum catalysts with ZnO as the support are being studied intensively [44-48].

The improvement of catalytic characteristics in hydrogenation and dehydrogenation reactions is commonly attributed to the formation of a Pt-Zn alloy upon reduction of Zn(II) in the presence of platinum [22, 44]. It is believed that the interaction between these metals and changes in the electronic state of platinum weaken the Pt-(C-C) bond, thus facilitating the desorption of olefins [49]. A further investigation of the adsorption of ethylene and formaldehyde on Pt, $Pt_3Zn$ and PtZn [49] confirmed a weaker adsorption of olefins and carbonyl compounds on bimetallic particles. One of the approaches to revealing the nature of platinum-zinc interaction is the deposition of these metals on a relatively inert carbon support [22, 50-51]. Thus, the formation of bimetallic PtZn particles was observed in the catalyst that showed a high activity in the dehydrogenation of isobutane with 100% selectivity for isobutylene [25]. Pt-Zn/C catalysts also showed a much higher activity and stability in the oxidation of $BH_4$ as compared with Pt/C. A study with variation of the zinc content demonstrated that a catalyst of the composition $Pt_{67}Zn_{33}$/C had the maximum activity [50]. The effect of zinc on the properties of platinum catalysts already containing tin as a promoter was reported [52-53]. The introduction of zinc into Pt-Sn/ZSM-5 increased the selectivity for propylene in propane dehydrogenation [52]. Zn addition to the PtSnK/γ-$Al_2O_3$ catalyst not only increased the platinum dispersion but also decreased coking of the surface in the dehydrogenation of isobutane. The authors of [56] suggest that the presence of zinc enhances the interaction of tin with the support and inhibits the process of tin reduction.

It should be noted that, unlike in the works [16-21, 54-56] where platinum was anchored by impregnation of the calcined LDH with toluene solutions of acetylacetonate platinum, in this study the maximum interaction of platinum with the modifying cation was provided by platinum anchoring via intercalation of Pt(IV) anionic chloride complexes into the interlayer space of zinc-containing LDH. This

anchoring method made it possible to use aqueous solutions of the metal complex. The authors of [57-59] tried to anchor the active metal via its interaction with a hydroxide precursor of the support. In [57], platinum was introduced as $Pt(acac)_3$ or $H_2Pt(OH)_6$ during the synthesis of ZnAl-LDH by the sol-gel method. However, this did not provide the anchoring of platinum from the acetylacetonate precursor; the introduction of $H_2Pt(OH)_6$ did not produce any changes in the structural parameters and gave no grounds to make a conclusion on platinum localization. In [58, 59], intercalation of metal complexes was performed under hydrothermal conditions, which led to significant changes in the chemical composition of the complexes.

In this work, anionic platinum complexes were anchored using the activated LDH species (LDH-OH) whose interlayer space was filled mostly with the charge compensating $OH^-$ anions. These anions possess better exchange properties than carbonate anions intercalating into the interlayer space directly during the LDH synthesis [14, 60]. Upon interaction of chloroplatinate with LDH-OH, the interlayer $OH^-$ ions are readily substituted by the doubly charged complex anions $[PtCl_6]^{2-}$. An additional driving force of this process is the neutralization of interlayer $OH^-$ anions by hydrogen ions of chloroplatinic acid. In this case, chloroplatinate is anchored via electrostatic interaction with the positively charged LDH layers without noticeable changes in the composition and symmetry of the complex [14].

## 2. Experimental

### *2.1. Catalyst preparation*

The synthesis of the layered hydroxides having different composition and carbonate counter ions was described in detail in [1-5, 13-15, 40]. The synthesis procedure included coprecipitation of $Mg^{2+}$, $Zn^{2+}$ and $Al^{3+}$ hydroxides from aqueous solutions (1 mol/L) of nitrate salts upon their interaction with the solutions containing carbonate and hydroxide ions (1 mol/L). The molar ratio of cations $(Mg^{2+}+Zn^{2+})/Al^{3+}$ in the salt solution was maintained constant and equal to 2. The variable fraction of zinc ions in the composition of bivalent cations $Zn^{2+}/(Mg^{2+}+Zn^{2+})$ was 0, 0.05, 0.1,

0.2, 0.5, 0.7, 1.0. These values were then used to denote the synthesized samples. The synthesis was carried out at pH = 10 and a temperature of 333 K. The resulting precipitates of layered hydroxides with interlayer carbonate anions Mg(Zn)Al-$CO_3$ were washed and dried for 16 h at 353 K. To obtain samples of activated LDH, i.e. those containing mostly the interlayer $OH^-$ anions (Mg(Zn)Al-OH), the initial (Mg(Zn)Al-$CO_3$) support was calcined at 823 K and hydrated once more in distilled degassed water. The calcination temperature was chosen from thermal analysis data and corresponded to a complete formation of the oxide phase. The hydration of mixed oxide led to restoration of the LDH layered structure (the memory effect) with appropriate changes in the composition of the interlayer space [13-15].

Chloroplatinic acid (Aurat Ltd., Specs. 6-09-2026-87) was adsorbed from an excess of aqueous solutions on the Mg(Zn)Al-OH support via the exchange of interlayer $OH^-$ anions with $[PtCl_6]^{2-}$ anions [14, 60]. Prior to physicochemical examination, hydroxide precursors of the supports were calcined at 823 K, and LDH with the deposited complexes (Mg(Zn)Al-$PtCl_6$) were calcined and reduced by hydrogen at 823 K. As a result, the Pt/Mg(Zn)$AlO_x$ samples with the platinum content of 0.3 and 1.0 wt.% were obtained. The concentrations of magnesium, zinc, aluminum and platinum in the initial solutions and solid samples after their dissolution were determined by inductively coupled plasma atomic emission spectrometry on a Varian 710-ES instrument.

*2.2. Characterization*

Data on the phase composition of layered hydroxides Mg(Zn)Al-$CO_3$, Mg(Zn)Al-OH, Mg(Zn)Al-$PtCl_6$ and the corresponding oxide phases were obtained on a D8 Advance (Bruker) diffractometer with monochromatized Cu-$K_\alpha$ radiation at 2θ diffraction angles between 5 and 80°, a scanning step of 0.05°, and a signal accumulation time of 5 s/step.

The nitrogen adsorption-desorption isotherms at 77.4 K were measured using an ASAP-2020 (Micromeritics) static volumetric apparatus. Prior to measurements,

the samples were evacuated at 573 K for 6 hours. A range of equilibrium relative pressures was between $10^{-3}$ and 0.996 $P/P_0$. The BET specific surface area ($S_{BET}$) was calculated from the adsorption isotherm at equilibrium relative values of nitrogen vapor $P/P_0$ = 0.05-0.25.

The measurements of carbon dioxide adsorption were made on a Sorptomatic-1900 automated static vacuum apparatus. Before measurements, the samples were treated in vacuum ($10^{-2}$ mm Hg) at 573 K. The isotherm of carbon dioxide adsorption obtained at P = 1 atm and a temperature of 303 K was used to calculate the total capacity of a sample with respect to this gas (physically and chemically adsorbed $CO_2$). After that, the sample was evacuated to $10^{-2}$ mm Hg at the same temperature for 1 hour to remove physically adsorbed molecules, and the second isotherm was obtained. The difference between two isotherms in the amount of adsorbed $CO_2$ made it possible to determine its part that was retained on the surface due to its chemical features [61, 62]. To assess the strength of basic sites, they were evacuated at 373, 473, and 573 K.

The reduction dynamics of the oxidized platinum species supported on mixed oxides Pt/Mg(Zn)$AlO_x$ was studied by the temperature-programmed reduction (TPR) on an AutoChem-2920 (Micromeritics) chemisorption analyzer. The samples obtained by calcination of LDH with the anchored platinum chloride complexes in air at 823 K were employed for TPR. TPR was carried out up to 823 K with a 10°C/min ramp rate using a 10% vol. $H_2$–Ar gas mixture (flow rate of 30 mL/min). Platinum dispersion in the reduced samples was estimated by pulse chemisorption of $H_2$ and CO probe molecules at room temperature assuming the stoichiometry of [Pt] : [H] = 1:1, [Pt] : [CO] = 1:1.

Micrographs of LDH were obtained on a scanning electron microscope JSM-6460 LV (JEOL Ltd.). To decrease the charging effect, the samples were coated with a conductive gold film ~20 nm in thickness. Samples of the platinum catalysts were examined by transmission electron microscopy (TEM). TEM images were obtained on a JEM-2010 (JEOL Ltd.) electron microscope. Local Energy Dispersive X-ray

(EDX) microanalysis was made on PHOENIX EDAX analyzer. Semi quantitative calculations of compositions were made with the software support of analyzer. Dark-field images (STEM-HAADF) were taken on a JEM-2200FS (JEOL Ltd.) electron microscope at 200 kV. The samples were prepared by depositing the ethanol suspension of samples powder on a copper grid that was covered with thin perforated carbon film.

X-ray photoelectron spectra (XPS) were recorded using a SPECS (Germany) spectrometer equipped with several isolated vacuum chambers for fast loading of samples, their thermal treatment and analysis. Samples were transferred between the chambers so as to prevent contacting air. Photoelectron spectra of samples were reproduced in the analyzer chamber at a pressure of $5\times10^{-9}$ Torr. For each sample, spectra were recorded using Mg$K_\alpha$ ($h\nu$ = 1253.6 eV) and Ag$L_\alpha$ ($h\nu$ = 2984.3 eV) radiation. The binding energy scale of spectrometer was calibrated against the lines of metallic gold and copper, Au4$f_{7/2}$ = 84.0 eV and Cu2$p_{3/2}$ = 932.6 eV. For any radiation, the spectra of non-conducting samples were calibrated against the C1*s* line whose binding energy was taken equal to 284.8 eV. Before the measurements the samples were pre-reduced in a hydrogen stream in a special quartz reactor and then transferred to a spectrometer in a short-term contact with air. No additional reduction treatment in the spectrometer was performed.

X-ray absorption measurements were performed at the beamline ID26 of the European Synchrotron Radiation Facility (Grenoble). The energy of X-ray incident beam was selected using the reflection from a double Si[111] crystal monochromator. Rejection of higher harmonics was achieved by two Si mirrors with Pd and Cr layers located at 2.5 mrad angle relative to the incident beam. The energy calibration was performed using a Pt metal foil sample. Pt$L_3$ EXAFS spectra were measured with the X-ray emission spectrometer at 12 K. The spectra at the $L_3$-edge were obtained by recording the intensity of the Pt $L_{\alpha1}$ emission line as a function of the incident energy. The emission energy was selected using the 660 reflection of

four spherically bent Ge crystal analyzers (with R = 1m). The local environment of Pt atoms was simulated for data filtered by the Fourier method ($\Delta R$ = 1–3 Å) with $k^2$ weighing ($k^2\chi(k)$ Pt$L_3$) within the wave vector range of $\Delta k$ = 3 – 11 $Å^{-1}$ ($T$ = 12 K) and using the EXCURV 98 program [63]. In data processing, the phase and amplitude characteristics were calculated in the von Bart and Hedin approximation. The amplitude suppression $S_0^2$ due to multielectron processes was determined for a Pt metal foil and then the obtained value ($S_0^2$ = 0.82) was set and fixed during simulation of the spectra of the studied samples. The Debye-Waller factors for interatomic distances from Pt atoms $2\sigma^2$(O; Mg) = 0.006 and $2\sigma^2$(Zn; Pt) = 0.01 were obtained from specific simulation variants (fits) and then fixed for the samples under consideration.

*2.3. Condition of propane dehydrogenation*

Dehydrogenation of propane was carried out in a flow-type reactor with a stationary catalyst bed (a 0.5 g loading) at a temperature of 823 K, atmospheric pressure, molar ratio $H_2/C_3H_8$ = 0.25, and weight hourly space velocity of 8 g/($g_{cat}$·h). Conditions of the catalyst pretreatment included calcination in air at 823 K and reduction in flowing hydrogen at 823 K. The time of each experiment was 5 h. The composition of products was analyzed on-line using a Khromos GH-1000 gas chromatograph equipped with an Rt-Alumina PLOT column (the length of 50 m) and a flame ionization detector. Deactivation parameters (DP) of catalysts [64] were calculated by the formula DP = ($x_{init} - x_{fin}$) · 100%/$x_{init}$, where $x_{init}$ and $x_{fin}$ are propane conversions after 0.5 and 5 h of the reaction.

At the steady-state conditions, the propane conversions were relatively low (the maximum conversion ~ 20 %) and the catalytic reactor was considered as a differential one. The reaction turnover frequency for the formation of propylene (TOF) and rate normalized per 1 g of catalyst were calculated according to equations:

$$TOF\left[\mathrm{mol}(C_3H_8)/(\mathrm{mol}_{Pt}\times \mathrm{h})\right] = r/(10^3 C_{Pt}) \quad (1)$$

$$r\left[\mathrm{mmol}(C_3H_8)/(g_{cat}\times h)\right]=10^3 WHSVx/M \quad (2)$$

where x – propane fraction dehydrogenated to propylene with participation of Pt sites, M – the molecular weight of propane, $C_{Pt}$ – concentration of platinum active sites (mol/g). The last parameter was calculated from Pt loading in catalysts and the dispersions:

$$C_{Pt}=\omega_{Pt}D_{Pt}(CO)/(100A_{Pt}) \quad (3)$$

$\omega_{Pt}$ – platinum content in the sample (wt. %), $A_{Pt}$ – the atomic weight of platinum, $D_{Pt}(CO)$ – dispersion of platinum determined by the pulse chemisorption of CO.

## 3. Results and Discussion

### *3.1. Properties of Mg(Zn)Al LDH and the corresponding mixed oxides*

The synthesis of LDH by coprecipitation of the hydroxides of bi- and trivalent metals from solutions of their salts used in this study can be described by the following chemical reaction (for the ratio $M^{2+}$: $Al^{3+}$ = 2):

$2\ M^{2+} + Al^{3+} + 6\ OH^- + 1/2\ (CO_3)^{2-} + mH_2O \rightarrow M^{2+}{}_2Al^{3+}(OH)^-{}_6[(CO_3)^{2-}{}_{1/2}\bullet mH_2O]$.

This synthesis method was chosen for its simplicity, high efficiency, and purity of the resulting products. Results of the chemical analysis of LDH samples after their calcination and dissolution showed (Table 1) that the obtained atomic ratios $Zn^{2+}/(Mg^{2+}+Zn^{2+})$ and $(Mg^{2+}+Zn^{2+})/Al^{3+}$ were close to the calculated values.

A SEM study of LDH with different cationic composition showed that the introduction of zinc changes surface morphology of the samples. The MgAl-OH LDH are the superimposed oval or hexagonal plates (Fig. 1a), which are typical of LDH with such composition [65]. The introduction of zinc cations decreases the size of the plates, alters their shape, and produces a denser packing (Fig. 1b, c).

According to XRD, the diffraction patterns of all the synthesized LDH samples are characterized by a series of 003 and 006 basal reflections as well as by the

peaks {*0kl*}: 012, 015, 018; {*hk0*}: 110 and 113 (Fig. S1a), which correspond to the hydrotalcite structure (No. 22-700, ICDD, PDF-2). This structure is present over the entire range of Zn/(Mg+Zn) ratios, but at a high zinc content the formation of an additional ZnO phase is observed. It is known that hydroxo compounds of zinc are thermally unstable, and their dehydration with the formation of the oxide phase may occur even upon drying at 313-333 K [66].

The main structural characteristics of Mg(Zn)Al-$CO_3$ samples are listed in Table 2. As the molar fraction of Zn increases, the lattice parameter *a*, which depends on the cationic composition of octahedral brucite-like layers, increases monotonically [1]. This result is caused by an increase in the fraction of $Zn^{2+}$, having a somewhat greater ionic radius: (R(Zn) = 0.074 nm and R(Mg) = 0.072 nm [67]), and confirms the intercalation of zinc cations into the LDH structure. Minor changes in the lattice parameter *c* are also observed, indicating a close composition of the interlayer space and an increase in the crystallite sizes in all directions ($L_c$ and $L_a$).

In order to obtain the oxide phase, the samples were calcined at 823 K. Such conditions provide a complete destruction of the LDH layered structure [40] with the removal of interlayer water and charge compensating anions. The diffraction patterns of the magnesium-aluminum sample and the samples containing a minimum amount of zinc (Fig. 1Sb) show the reflections that are assigned in the literature to the periclase-type MgO phase or the layered defect spinel [68]. However, with increasing the zinc content, the structure of the oxide phase changes and transforms into the defect wurtzite-like hexagonal structure. Microstructural characteristics of the calcined samples are listed in Table 1S.

The defect wurtzite-like oxide, similar to the layered defect spinel in the case of magnesium-containing samples, can be hydrated in water with restoration of the hydrotalcite structure (the memory effect) [40]. However, a part of zinc is not embedded in restoration, and the fraction of zinc oxide in the activated Mg(Zn)Al-OH samples increases in comparison with the initial Mg(Zn)Al-$CO_3$ samples. Thus, for Mg(Zn)Al-OH-0.7, the fraction of ZnO was 10 rel. %. The ZnO phase remains also in

the final Pt/Mg(Zn)$O_x$ samples, thus producing some nonuniformity of zinc distribution over the surface.

TEM study of the sample with a rather high content of zinc, Zn/(Mg+Zn) = 0.5, revealed the presence of not only the spinel-like phase, but also the other phase (Fig. 2 marked by arrows) which is likely related to the zinc oxide. To verify two regions were selected, only one of which contained particles of the second phase (Fig. 2, region 1). The performed EDX-microanalysis of selected surface regions revealed the presence of not only the oxide phase with the calculated composition (Fig. 2, region 2) but also the zinc-enriched phase (Fig. 2, region 1) with the (Mg+Zn)/Al ratio substantially exceeding the calculated value. This result agrees well with XRD data for the oxide phase. The XPS study also showed the surface enrichment with zinc for some samples (Table 1).

The shape of the hysteresis loop on the nitrogen adsorption-desorption isotherms obtained for the mixed oxide samples under consideration (Fig. 3a) allows their attribution to the IV type isotherm with the hysteresis loop H3, according to the IUPAC nomenclature. It should be noted that the isotherms for $ZnAlO_x$ and Mg(Zn)$AlO_x$-0.7 samples have two separate hysteresis loops at relative pressures $P/P_0$ = 0.4-0.57 and 0.85-0.99 (Fig. 3a, the insert). The presence of an additional loop in the low-pressure region may be related to quite a high content of the ZnO phase having a proper porosity in these samples.

A comparison of the textural characteristics listed in Table 3 shows that the $MgAlO_x$ sample has the highest specific surface area equal to 287 $m^2$/g. As the zinc fraction in the composition of bivalent cations increases, the $S_{BET}$ value gradually decreases and at a Zn/(Mg+Zn) ratio of 0.5 and 0.7 becomes as low as 170-150 $m^2$/g. The $V_{ads}$ values remain constant up to Zn/(Mg+Zn) = 0.7. A sharp decrease in

the adsorption volume for Mg(Zn)$AlO_x$-0.7 and $ZnAlO_x$ samples is also related to their phase inhomogeneity. The $ZnAlO_x$ sample with the maximum content of zinc oxide has the least developed pore structure: its specific surface area is 111 $m^2/g$, and $V_{ads}$ = 0.20 $cm^3/g$, which is much lower as compared with magnesium-aluminum oxide.

Analysis of PSDC (Fig. 3b) shows that the pore space of $AlMgO_x$ and samples with a minimum content of zinc is formed mostly by mesopores with the diameter of 5-40 nm (up to 70%). An increase in the zinc fraction to 0.2 and 0.5 increases the contribution of large mesopores and macropores. The contribution of pores with the diameter greater than 40 nm becomes prevailing for these systems (70-80%). In the samples with a maximum zinc content (including zinc in ZnO), a growth of the fraction of small mesopores (up to 5 nm) is observed, which leads to bimodality of PSDC and agrees with the shape of adsorption-desorption isotherms for these samples (Fig. 3a, the insert).

The effect of zinc introduction into the structure of LDH and, accordingly, into the oxide supports on their basic properties was studied using the adsorption of $CO_2$ [64, 65]. As follows from data in Fig. 4, the partial or complete substitution of Mg by Zn considerably deteriorates the ability of the obtained oxides to chemisorb the $CO_2$ probe molecules. When evacuation was performed at a low temperature (303 K), a greater capacity with respect to $CO_2$ (0.5) was observed for the $MgAlO_x$ and Mg(Zn)$AlO_x$ samples. Under more severe evacuation conditions, $CO_2$ desorption from the surface of zinc-containing samples became more pronounced. The revealed distinctions can be attributed to the presence of a greater amount of stronger basic sites in $MgAlO_x$, which can confine $CO_2$ molecules at high temperatures of evacuation [69]. However, the Mg(Zn)$AlO_x$-0.5 sample, which contains both bivalent metals, has a considerable amount of weakly basic sites. Thus, the replacement of Mg by Zn in LDH decreases the amount of basic sites in the mixed oxide, especially the amount of the most basic sites that confine $CO_2$ at the evacuation temperatures of 373-573 K.

*3.2. The formation and properties of supported platinum*

In order to obtain supported platinum Pt/Mg(Zn)AlO$_x$ catalysts, the Pt(IV) chloride complexes were anchored on the activated LDH species via the anionic exchange with interlayer $OH^-$ anions. The anchoring process, adsorption capacity of LDH and composition of supported complexes were described in detail in our earlier works [14, 60]. As a result of intercalation, the structure of LDH is preserved; however, the crystallite sizes slightly decrease along all directions. Thus, Table 2 shows an increase in the lattice parameter *c* for Mg(Zn)Al-[$PtCl_6$]-0.2 upon anchoring of larger chloroplatinate anions in the case of their predominant localization in the interlayer space of LDH. In the process, the lattice parameter *a* remains virtually constant, which testifies to stability of the brucite layers and invariability of their chemical composition during the ionic exchange [1].

The Mg(Zn)Al-[$PtCl_6$] LDH samples with the anchored platinum chloride complexes were subjected to oxidative treatment at a temperature of 823 K, which is sufficient for the formation of the oxide support and supported platinum oxide species. After that, the obtained samples were reduced in flowing hydrogen at 823 K, which is the temperature of the test reaction. The platinum content in the synthesized catalysts was close to 0.3 wt. % (Table 4). The formation of platinum sites from the platinum oxide species in the course of reductive treatment was examined by means of TPR followed by measuring the dispersion of supported platinum.

Figure 5 shows that the introduction of zinc strongly changes the reduction process: as the zinc content in the support increases, the temperature of the maximum hydrogen absorption on the TPR profiles monotonically decreases from 603 K (for the magnesium-aluminum support) to 443 K (for the aluminum-zinc support). The shift of hydrogen absorption regions toward low temperatures can be related to lowering the interaction strength of platinum oxide species with the support due to changes in its composition (an increase in the zinc content). At the same time, calcination of LDH with the anchored platinum complexes may be accompanied by

the formation of supported oxide species of different composition, where zinc cations are present in the chemical environment of platinum and their amount increases with the zinc content of the support. This may change the temperature conditions for the reduction of these particles.

It is known that zinc oxide is reduced quite readily in a hydrogen medium [70], and the presence of platinum catalyzes this process. Thus, ZnO in the composition of Pt/ZnO can be reduced to metallic zinc with the formation of a PtZn alloy at 473 K [44]. The study of Pt/ZnO [47] demonstrated that the regions of platinum and zinc reduction overlap each other: on the TPR profile, the hydrogen consumption region of 373-503 K was assigned to the reduction of oxidized platinum species, and the temperature range of 453-553 K corresponded to the reduction of ZnO contacting with platinum. Comparing the TPR data for alumina-supported Pt, Zn–Pt and Zn, the authors of [71] also concluded that platinum and zinc are reduced in the same temperature region, and the presence of platinum substantially increases the amount of reduced zinc and hence the amount of absorbed hydrogen. A similar result was obtained in [22] by analysis of TPR profiles of PtZn/C catalyst. The hydrogen consumption peak corresponding to the joint reduction of ZnO and platinum oxychlorides was recorded at 546 K. Therewith, the amount of hydrogen absorbed during TPR of the zinc-containing catalyst was greater as compared with the case of its monometallic analog.

The TPR data obtained in our study agree with the results described above [22, 72]. The presence of a single broad peak on TPR profiles and the hydrogen absorption exceeding the stoichiometric amount for the reaction $Pt^{4+} \rightarrow Pt^{o}$ can also be attributed to the reduction of platinum and to the partial reduction of zinc that occurs in a close temperature range.

In the reduced catalysts, the dispersion of platinum particles was estimated by measuring the amount of chemisorbed $H_2$ and CO molecules, taking into account the adsorption stoichiometry H(CO)/Pt = 1. We used two types of probe molecules similar to [72]. The study of PtZn/H-mordenite catalysts [72] revealed that CO

molecules (in distinction to $H_2$) can be adsorbed on zinc particles, which may give overestimated results in the calculation of platinum dispersion and indicate a pronounced reduction of zinc.

As follows from Table 4, the values of dispersion obtained for all the samples after their reduction at 823 K are virtually independent of the features of a probe molecule, thus testifying to the absence of a noticeable amount of individual particles of reduced zinc on the catalyst surface. For all the tested catalysts, low dispersions of supported platinum were observed, and the introduction of zinc into support produced an additional decrease in the dispersion.

In some studies [15, 73-76], the anomalously low dispersions of platinum on magnesium-containing supports were attributed to the platinum interaction with basic sites that altered its adsorption properties. In these studies, an essential difference was observed between particle sizes estimated by electron microscopy and those calculated from chemisorption of probe molecules (not related to blocking of the active surface of platinum) [15, 73-76].

A similar result was reported in the study devoted to the effect of zinc on the properties of Pt/MCM-41 [77]. It was shown that the introduction of zinc into the silicate (2-4% Zn) simultaneously with platinum or in advance essentially modified physicochemical properties of the supported platinum. Hydrogen chemisorption was suppressed and the H/Pt ratio decreased from 0.9 to 0.01. The measurement of differential heats of $H_2$ adsorption on these platinum catalysts revealed a considerable decrease (from 80 to 53 kJ $mol^{-1}$) even at the minimum zinc content. The hydrogenating activity of platinum in the transformation of croton aldehyde at 80°C also showed a significant decrease.

A discrepancy between the adsorption data and the particle sizes estimated by electron microscopy was found also for the systems examined in our work. Electron microscopy data for the samples of platinum catalysts prepared with $MgAlO_x$ and $Mg(Zn)AlO_x$-0.5 supports (samples with the platinum content of 1 wt. % were used) are depicted in Fig. 6. It should be noted that platinum particles in the zinc-containing

samples had a low contrast in the TEM study (Fig. 6b), probably due to significant changes in their morphology upon anchoring on the supports of the indicated composition; therefore, sizes of the platinum particles were estimated in the STEM-HAADF mode.

According to Fig. 6, platinum in the tested samples is present as isolated and highly dispersed particles of quite a uniform size. The introduction of zinc decreases the particle size of supported metal. The average diameter of the particles decreases from 1.9 nm (for 1%Pt/MgAl$O_x$) to 1.5 nm (for 1%Pt/Mg(Zn)Al$O_x$-0.5), which corresponds to the platinum dispersion of 60 and 75%, respectively. The zinc-containing sample (in distinction to magnesium-aluminum system) contains metal particles with the diameter smaller than 1 nm, while the fraction of particles with the diameter greater than 2 nm is insignificant. The data obtained give grounds to suppose that the low dispersions, as determined by CO and $H_2$ chemisorption, are related to the effect of the support nature on the adsorption properties of supported platinum, and further catalytic measurements showed that the presence of zinc in the support changes both the adsorption and the catalytic properties of platinum.

The effect of zinc in the composition of oxide support on the catalytic properties of supported platinum was revealed using the propane dehydrogenation reaction. The chosen reaction conditions (a moderate temperature, high dilution with hydrogen, and low weight of the sample) prevent fast deactivation of the catalyst and make it possible to assess the dehydrogenating activity of platinum and compare the catalysts without approaching the equilibrium value of propane conversion.

Investigation of the synthesized catalysts showed that all the Zn-containing samples at the lower platinum dispersions obtained by chemisorption method possess a higher dehydrogenating activity in comparison with the magnesium-aluminum system. Figure 7 displays the propane conversions after 4 hours of the catalyst operation. The highest conversion, 20%, is observed for the sample with a Zn/(Mg+Zn) ratio in the support equal to 0.1. For other Zn-containing samples, the

conversions fall in the range of 11-15%, and the conversion for Pt/AlMg$O_x$ under the same conditions of testing does not exceed 7%.

Selectivity for the formation of propylene as the target product is high for all the tested samples and reaches 98.5-99.3% (Fig. 7). Somewhat lower values of this parameter for the samples with bimetallic supports Pt/AlMg$O_x$ and Pt/AlZn$O_x$ are related to a greater contribution of the hydrogenolysis of C-C bonds over these catalysts (Fig. S2a). In addition, due to a higher surface acidity of the aluminum-zinc sample, the formation of products with a high molecular weight is more pronounced (Fig. S2b). This results in fast deactivation of the Pt/AlZn$O_x$ sample, which has a high initial activity (conversion 19%). The deactivation reaches 30%, which is nearly fourfold greater as compared with more basic Mg-containing samples. It should be noted that deactivation under these conditions is even more pronounced for the 0.3%Pt/$Al_2O_3$ catalyst (above 40%), and the yield of $C_1$-$C_2$ and $C_{4+}$ by-products exceeds the values obtained for the least basic Pt/AlZn$O_x$ by a factor of 2-3.

Thus, analysis of differences in the catalytic properties of Pt/MgAl$O_x$ and Pt/Mg(Zn)Al$O_x$ samples shows that the modifying action of zinc manifests itself as an increase in the activity of Zn-containing platinum catalysts toward propane conversion at a high selectivity for propylene over the entire time of experiment. Therewith, the presence of magnesium increases the catalyst stability by suppressing the reactions that involve acidic sites of the support.

A higher activity of the sample with Zn/(Mg+Zn) = 0.1 may be related to the optimal state of the metallic site that is formed on the support of the indicated composition. We showed that this support has a high phase homogeneity, a developed surface area and quite a high basicity. Most likely, such parameters of the support can ensure a high dispersion of supported metal particles, and the zinc content is sufficient to create a necessary Zn/Pt ratio in the active site and an optimal electronic state of platinum. In some works [26, 64, 49, 53], the promoting action of zinc is attributed mostly to a decrease in the size of platinum ensembles (the geometric effect). The active site of dehydrogenation is represented by a single

platinum atom, and the hydrogenolysis and coke formation reactions require the presence of larger platinum particles; so, a decrease in the size of platinum particles leads to the suppression of side reactions. Some authors discuss the electronic (ligand) effect of zinc, i.e. an increase in the electronic density of platinum upon formation of bimetallic PtZn particles [22, 44, 77, 78], which provides the necessary adsorption characteristics of the catalyst.

An XPS study was carried out to reveal the state of supported platinum and the nature of its increased activity in the catalysts synthesized from Zn-containing LDH. Samples with the platinum content of 1 wt. % and the ratio of Zn/(Mg+Zn) = 0, 0.1, 0.5, 0.7 were investigated (Fig. 8 and Table 1). These samples were synthesized by the same procedure as the low-loading platinum catalysts that were tested in dehydrogenation of propane. The main steps of the synthesis were the intercalation of platinum complexes in the interlayer space of LDH and the subsequent oxidative and reductive treatments at 823 K.

The XPS method is quite informative for investigating the electronic state of the surface of heterogeneous catalysts; however, its application to platinum catalysts with the supports containing aluminum atoms has a significant limitation related to superposition of the most intense Pt4*f* line of platinum and the spectral Al2*p* line of the support when using X-ray tubes with Al or Mg anodes [79, 80]. However, at a harder Ag$L_\alpha$ radiation with the energy $h\nu$ = 2984.3 eV, the most intense lines in XP spectra are Al1*s* with the binding energy $E_b \approx 1560$ eV and Pt3$d_{5/2}$ with $E_b \approx 2122$ eV. This eliminates the problem of mutual overlap of the lines of active component and support. Therewith, monochromatization strongly decreases the halfwidth of the initially broad Ag$L_\alpha$ line and allows a reliable interpretation of the electronic state of platinum: for the metal, $E_b$ = 2121.8 eV; for $Pt^{2+}$ ($K_2PtCl_4$), $E_b$ = 2123.5 eV; and for $Pt^{4+}$ ($K_2PtCl_6$), $E_b$ = 2125.3 eV [82]. Investigation of the other elements in the catalyst composition (Mg, Al, Zn) was performed using a conventional XPS technique with the Mg$K_\alpha$ source. Atomic ratios of the elements were calculated with the reference data reported in [81].

Analysis of the Pt3$d_{5/2}$ line for the tested samples showed that all spectra are symmetrical (FWHM is 3.2 - 4 eV) and well approximated by the deconvolution procedure using the standard program XPSPeak. Probably these spectral lines represent a single energy state of platinum and they are not superposition of several electronic states.

It should be noted that the spectra of Pt3d region (Fig. 8) in the side of higher binding energies contain low-intensity line which is absent for a sample 1 (without Zn) and increases as increase the proportion of zinc in the samples 2-4. This low-intensity line obtained as a result of deconvolution procedure cannot be conform to the platinum line because BE for platinum with maximum degree of oxidation $Pt^{4+}$ is significantly lower (2125.3 eV). This line apparently corresponds to Auger Zn-KLL [82].

The introduction of a large amount of zinc into the structure of support produced substantial changes in the electronic state of platinum: XPS spectra showed a pronounced shift of the Pt3$d_{5/2}$ band maximum toward low energies (Table 1 and Fig. 8). The obtained values of energy are close for the samples 1%Pt/Mg(Zn)$AlO_x$-0.5 and 1%Pt/Mg(Zn)$AlO_x$-0.7 (2121.4-2121.5 eV) and are somewhat lower than those found for the reduced metal species ($Pt^0$), 2121.8 eV. The observed effects cannot be attributed to substantial differences in the dispersion states of platinum, because the Pt/Al atomic ratio on the surface was close for all the studies samples and even increased monotonically with the increasing zinc content (Table 1). A possible explanation is the formation of bimetallic particles with the charge transfer from zinc to platinum. The possibility of their formation agrees with the TPR results and the decreased chemisorption of $H_2$ and CO probe molecules.

Structural parameters of such particles were determined by means of EXAFS, which is employed quite widely for investigation of supported catalyst and allows revealing the local structural parameters (the interatomic distances *R* and coordination numbers *N*) that are difficult to measure by other methods in the case of

systems having a limited long-range order, in particular, owing to the highly dispersed state of the objects under consideration. Figure S3a, b shows Pt$L_3$ EXAFS spectra and radial distribution functions of Pt$L_3$ EXAFS spectra of the samples 1%Pt/Mg(Zn)$AlO_x$ with Zn/(Mg+Zn) = 0, 0.1, 0.5, 0.7. Figure S3c shows good agreement between experimental and model EXAFS spectra. The local structure parameters (the interatomic distances (*R*) and partial coordination numbers (*N*) were determined in the simulation process ("fitting") of EXAFS data (Table 5).

Analysis of the acquired data (Table 5, Fig. S3) shows that a gradual increase in the zinc content of support essentially changes the composition of metallic sites of the catalyst. In the magnesium-aluminum sample, along with the Pt-Pt bonds, there are the Pt-O bond and the Pt-Mg(Al) distance, which may testify to the interaction of platinum particles with the support and the possibility to stabilize a part of platinum in the oxidized state due to incomplete reduction of supported Pt(IV) oxide species. This assumption agrees with the XPS data according to which a part of platinum in this sample is in the ionic state close to $Pt^{2+}$ even after the reduction at 823 K [14]. It should be noted that, since the Mg and Al atoms resided at approximately equal distances from the adsorbing atom and corresponded to the joint maximum on the radial distribution function, it was impossible to estimate the contributions of these elements. Their total amount (Al+Mg) at a distance of 2.9 Å from Pt was shown to be ~3 for magnesium-aluminum sample and ~2 for the other samples.

Even a minimum zinc content in the support leads to the appearance of the Pt-Zn bond. The Pt-Zn (R(Zn)) bond lengths are 2.67 and 2.57 Å, while the Pt-Pt (R(Pt)) distances are 2.85 and 2.78 Å for the samples with Zn/(Mg+Zn) = 0.05 and 0.1, respectively (Table 5). The obtained values agree well with the Pt-Zn and Pt-Pt distances in solid solutions of the composition $Pt_1Zn_1$ and $Pt_1Zn_{1.68}$ [85] (Table 5). At the same time, platinum atoms in these samples are bound mostly to the oxygen atoms, and the number of Pt-O bonds is greater than that of Pt-Pt bonds. This effect is attributed to the formation of flat platinum particles and/or their encapsulation by the support [84, 85]. In both cases, a high strength of the metal-support interaction is

observed. Thus, similar results were reported for the catalyst $Rh/La_2O_3$ [84]. Rhodium particles in this catalyst, according to electron microscopy data, had the size of 12-20 Å and were represented by thin plates on the support surface.

When going to samples with a higher zinc content, Zn/(Mg+Zn) = 0.5 and 0.7, oxygen in the coordination sphere of platinum virtually disappears, similar to the Pt-Pt distances (Fig. S3). A decrease in the coordination number with respect to oxygen characterizes a decrease in the interaction strength of platinum with the elements of support, which is corroborated by a significant decrease in the temperature of platinum reduction observed on TPR profiles (Fig. 5). Along with the decrease in N(O) and N(Pt) in these samples, the coordination number of Pt-Zn increases (N(Zn) for these samples is close to 11). Hence, platinum atoms in these samples are surrounded by Zn atoms. Such a change in the platinum environment may give rise to the interaction that increases the electronic density on platinum and alters its adsorption and catalytic properties. Exactly such a situation is likely to take place in the low-loading platinum catalysts where the Zn/Pt ratio should be quite high.

## 4. Conclusions

Zinc-containing LDH were synthesized in order to obtain the oxide support $Mg(Zn)AlO_x$, which can promote the dehydrogenating activity of supported platinum. It was found that the phase-homogeneous LDH and oxides can be produced if the fraction of zinc in the composition of bivalent metals Zn/(Zn+Mg) does not exceed 0.5. The presence of an additional zinc-enriched phase can strongly affect the textural parameters of the support by increasing the fraction of fine mesopores with the diameter smaller than 5 nm. In addition, this diminishes the basic properties of the support, thus initiating the reactions that yield products with a greater molecular weight under high-temperature conditions, and facilitating the catalyst deactivation.

The presence of zinc in the composition of support substantially affects the formation of supported platinum particles as well as the adsorption and catalytic properties of platinum. The reduction of platinum from the oxide species anchored on

the support and the partial reduction of zinc catalyzed by platinum lead to the formation of supported bimetallic particles whose composition and interaction with the support depend on the zinc content. Analysis of the data obtained by a set of methods allows a conclusion that the suggested approach to modification of platinum (a preliminary embedding of the modifying element into the structure of support) produces both the geometric and ligand effects. Implementation of the geometric effect is confirmed by an increase in the fraction of zinc atoms in the coordination sphere of platinum and by a decrease in the particle size of supported metal. This enhances the dehydrogenating activity of the catalyst and suppresses the hydrogenolysis of C-C bonds. The ligand effect manifests itself as changes in the electronic state of platinum. The presence of zinc stabilizes the main part of platinum in the active metallic state, and the shift of Pt3$d_{5/2}$ band toward lower energies suggests the possibility of interaction $Pt^{\delta-}$-$Zn^{\delta+}$. Such interaction may underlie both the observed low ability of platinum to chemisorb $H_2$ and CO probe molecules and the easier desorption of propylene as the target product, which is essential for maintaining a stable operation of the catalyst.

**Acknowledgements**

The authors are grateful to O.V. Maevskaya for participation in the catalyst preparation, N.N. Leont'eva and I.V. Muromtsev for the XRD experiments, T.V. Kireeva and A.V. Shilova for the chemical analysis of samples by AAS and ICP OES. We also thank A.N. Salanov (Boreskov Institute of Catalysis, Siberian Branch of the Russian Academy of Sciences) for affording the SEM micrographs.

## References

[1] Q. Wang, D. O'Hare, Chem. Rev. 112 (2012) 4124.

[2] B. Zümreoglu-Karan, A. Nedim Ay, 66 (2012) 1.

[3] J. Wang, L. Wang, X. Chen, Y. Lu, W. Yang, J Solid State Electrochem. 19 (7) (2015) 1933.

[4] G. Mascolo, M.C. Mascolo, Microporous and Mesoporous Mater. 214 (2015) 246.

[5] T. Selvam, A. Inayat, W. Schwieger, Dalton Trans. 43 (27) (2014) 10365.

[6] S. Nishimura, A. Takagaki, K. Ebitani, Green Chem. 15(8) (2013) 2026.

[7] S. He, Z. An, M. Wei, D. G. Evans, X. Duan, Chem. Commun. 49(53) (2013) 5912.

[8] G. Fan, F. Li, D. G. Evans, X. Duan, Chem. Soc. Rev. 43(20) (2014) 7040.

[9] T. Baskaran, J. Christopher, A. Sakthivel, RSC Adv. 5 (2015) 98853.

[10] J. Feng, Y. He, Y. Liu, Y. Du, D. Li, Chem. Soc. Rev. 44(15) (2015) 5291.

[11] D. Akporiaye, S.F. Jensen, U. Olsbye, F. Rohr, E. Rytter, M. Ronnekleiv, A.I. Spjelkavik, Ind. Eng. Chem. Res. 40 (2001) 4741.

[12] A. Virnovskaia, S. Jorgensen, J. Hafizovic, O. Prytz, E. Kleimenov, M. Havecker, H. Bluhm, A. Knop-Gericke, R. Schlogl, U. Olsbye, Surf. Sci. 601 (2007) 30.

[13] L.N. Stepanova, O.B. Belskaya, M.O. Kazakov, V.A. Likholobov, Kinet. Catal. 54 (2013) 505.

[14] O.B. Belskaya, T.I. Gulyaeva, V.P. Talsi, M.O. Kazakov, A.I. Nizovskii, A.V. Kalinkin, V.I. Bukhtiyarov and V.A. Likholobov, Kinet. Catal. 55 (2014) 786.

[15] O. B. Belskaya, L. N. Stepanova, T. I. Gulyaeva, D. V. Golinskii, A. S. Belyi, and V. A. Likholobov, Kinet. Catal. 56 (2015) 655.

[16] V. Galvita, G. Siddiqi, P. Sun, A.T. Bell, J. Catal. 271 (2010) 209.

[17] J. Wu, Z. Peng, A.T. Bell, J. Catal. 311 (2014) 161.

[18] P. Sun, G. Siddiqi, M. Chi, A.T. Bell, J. Catal. 274 (2010) 192.

[19] G. Siddiqi, P. Sun, V. Galvita, A.T. Bell, J. Catal. 274 (2010) 200.

[20] P. Sun, G. Siddiqi, W.C. Vining, M. Chi, A.T. Bell, J. Catal. 282 (2011) 165.

[21] J. Wu, Z. Peng, P. Sun, A.T. Bell, Appl. Catal. A., 470 (2014) 208.

[22] J. Silvestre-Albero, J.C. Serrano-Ruiz, A. Sepu´lveda-Escribano, F. Rodrı´guez-Reinoso, Appl. Catal. A 292 (2005) 244.

[23] J.M. Sinfelt, in: J.R. Anderson, M. Boudart (Eds.), Catalysis, Science and Technology, 1, Springer, Heidelberg, 1981, p. 257.

[24] G. Aguilar-Ríos, M. Valenzuela, P. Salas, H. Armendáriz, P. Bosch, G. del Toro, R. Silva, V. Bertín, S. Castillo, A. Ramírez-Solís, I. Schifter, Appl. Catal. A 127 (1995) 65.

[25] Z. Xu, Z.T.Y. Fang, L. Lin, Stud. Surf. Sci. Catal. 112 (1997) 42.

[26] S.B. Kogan, M. Herskowitz, Catal. Commun. 2 (2001) 179.

[27] S. de Miguel, A. Castro, O. Scelze, J.L.G. Fierro, J. Soria, Catal. Lett. 36 (1996) 201.

[28] P. Praserthdam, N. Grisdanurak, W. Yuangsawatdikul, Chem. Eng. J. 77 (2000) 215.

[29] R.D. Cortright, J.A. Dumesic, Appl. Catal. A 129 (1995) 101.

[30] R.D. Cortright, J.M. Hill, J.A. Dumesic, Catal. Today 55 (2000) 213.

[31] Y. Wang, Y. Wang, S. Wang, X. Guo, S.-M. Zhang, W.-P. Huang, S. Wu, Catal. Lett. 132 (2009) 472.

[32] G. Aguilar-Ríos, P. Salas, M.A. Valenzuela, H. Armendáriz, J.A. Wang, J. Salmones, Catal Lett. 60 (1999) 21.

[33] D. Akporiaye, S.F. Jensen, U. Olsbye, F. Rohr, E. Rytter, M. Rønnekleiv, A.I. Spjelkavik, Ind. Eng. Chem. Res. 40 (2001) 4741.

[34] M.M. Schubert, M.J. Kahlich, G. Feldmeyer, M. Hüttner, S. Hackenberg, H.A. Gasteiger, R.J. Behm, Phys. Chem. Chem. Phys. 3 (2001) 1123.

[35] J.L. Margitfalvi, I. Borbath, M. Hegedus, E. Tfirst, S. Gobolos, K. Lazart, J. Catal. 196 (2000) 200.

[36] A. Erhan Aksoylu, M.M.A. Freitas, J.L. Figueiredo, Catal. Today 62 (2000) 337.

[37] F. Coloma, A. Sepúlveda-Escribano, J.L.G. Fierro, F. Rodríguez-Reinoso, Appl. Catal. A 136 (1996) 231.

[38] V. Ponec, Appl. Catal. A 149 (1997) 27.

[39] N. Homs, J. Llorca, P. Ramírez de la Piscina, F. Rodríguez-Reinoso, A. Sepúlveda-Escribano, J. Silvestre-Albero, Phys. Chem. Chem. Phys. 3 (2001) 1782.

[40] O.B. Belskaya, N.N. Leontʹeva, T.I. Gulyaeva, S.V. Cherepanova, V.P. Talzi, V.A. Drozdov, V.A. Likholobov, Russ. Chem. Bull. 62 (2013) 2349.

[41] M. Bidaoui, C. Especel, S. Sabour, L. Benatallah, N. Saib-Bouchenafa, S. Royer, O.Mohammedi, J. Mol. Catal. A: Chem. 399 (2015) 97.

[42] A. Yarulin, C Berguerand., I. Yuranov, F. Cardenas-Lizana, I. Prokopyeva, L.Kiwi-Minsker, J. Catal. 321 (2015) 7.

[43] C. Berguerand, A. Yarulin, F. Cardenas-Lizana, J. Warna, E. Sulman, D.Yu. Murzin, L. Kiwi-Minsker, Ind. Eng. Chem. Res. 54(35) (2015) 8659.

[44] M. Consonni, D. Jokic, D.Y. Murzin, R. Touroude, J. Catal. 188 (1999) 165.

[45] J. Silvestre-Albero, F. Coloma, A. Sepúlveda-Escribano, F. Rodríguez-Reinoso, Stud. Surf. Sci. Catal. 135 (2001) 29.

[46] J. Silvestre-Albero, M.A. Sánchez-Castillo, R. He, A. Sepúlveda-Escribano, F. Rodríguez-Reinoso, J.A. Dumesic, Catal. Lett. 74 (2001) 17.

[47] A. Yarulin, C. Berguerand, A.O.Alonso, I. Yuranov, L. Kiwi-Minsker, Catal. Today 256 (2015) 241.

[48] M. Checa, F. Auneau, J. Hidalgo-Carrillo, A. Marinas, J.M. Marinas, C. Pinel, F. J. Urbano, Catal. Today 196 (2012) 91.

[49] Y. Changlin, X. Hengyong, G. Qingjie and L. Wenzhao, J. Mol.Catal. A: Chem. 266 (2007) 80.

[50] L. Yi, W. Wei, C. Zhao, C. Yang, L. Tian, J. Liu, X. Wang, Electrochim. Acta 158 (2015) 209.

[51] S. Ito, Y. Suwa, S. Kondo, S. Kameoka, K. Tomishige, K. Kunimori, Catal. Commun. 4 (2003) 499.

[52] N. Zeeshan, T. Xiaoping, F. Wei, Korean J. Chem. Eng. 26 (2009) 1528.

[53] Y. Zhang, Y. Zhou, J. Shi, X. Sheng, Y. Duan, S. Zhou, Z. Zhang, Fuel Process. Technol. 96 (2012) 220.

[54] E. Redekop, V. Galvita, H. Poelman, V. Bliznuk, C. Detavernier, G. Marin, ACS Catal. 4 (2014) 1812.

[55] M. Filez, E.A. Redekop, H. Poelman, V.V. Galvita, R.K. Ramachandran, J. Dendooven, C. Detavernier, G.B. Marin, Chem. Mater. 26 (2014) 5936.

[56] S. Albertazzi, G. Busca, E. Finocchio, R. Glöckler, A. Vaccari, J. Catal. 223 (2004) 372.

[57] D. Tichit, O. Lorret, B.Coq, F. Prinetto, G. Ghiotti, Microporous Mesoporous Mater. 80 (2005) 213.

[58] P. Beaudot, M.E. De Roy, J.P. Besse, J. Solid State Chem. 177 (2004) 2691.

[59] P. Beaudot, M. E. De Roy, J. P. Besse, J. Solid State Chem. 161 (2001) 332.

[60] O.B. Belskaya, T.I. Gulyaeva, N.N. Leont'eva, V.I. Zaikovskii, T.V. Larina, T.V. Kireeva, V.P. Doronin, V.A. Likholobov, Kinet. Catal. 52 (2011) 876.

[61] S.S. Nam, H.K. Kim, G. Ishan, M.J. Choiane, K.W. Lee, Appl. Catal. A 179 (1999) 155.

[62] R. Salvador, B. Casal, M. Yates, M.A. Martin-Luengo, E. Ruiz-Hitzky, Appl. Clay Sci. 22 (2002) 103.

[63] N. Binsted, EXCURV98, CCLRC Daresbury Laboratory Computer Program, 1998.

[64] Y. Wang, Y. Wang, S. Wang, X. Guo, S.M. Zhang, W.P. Huang, S. Wu, Catal. Lett. 132 (2009) 472.

[65] Q. Wang, H.H. Tay, Z. Guo, L. Chen, Y. Liu, J. Chang, Z. Zhong, J. Luo, A. Borng, Appl. Clay Sci. 55 (2012) 18.

[66] A.S. Shaporev, Dokl. Chem. (Engl. Transl.) 426 (2009) 194.

[67] R.D. Shannon, Acta Cryst. A32 (1976) 751.

[68] S.V. Cherepanova, N.N. Leont'eva, A.B. Arbuzov, V.A. Drozdov, O.B. Belskaya, N.V. Antonicheva, J. Solid State Chem. 225 (2015) 417.

[69] J.I. Di Cosimo, V.K. Díez, M. Xu, E. Iglesia, C.R. Apesteguía, J. Catal. 178 (1998) 499.

[70] S.-W. Park, O.-S. Joo, K.-D. Junga, H. Kim, S.-H. Han, Appl. Catal. A 211 (2001) 81.

[71] C. Yu, H. Xu, Q. Ge, W. Li, J J. Mol.Catal. A: Chem. 266 (2007) 80.

[72] M.M. Ramirez-Corredores, T. Romero, M. Gonzalez, Stud. Surf. Sci. Catal. 130C (2000) 2507.

[73] S.A. Bocanegra, A. Guerrero-Ruiz, O.A. Scelza, S.R. de Miguel, Catalysis in Industry. 5 (2012) 63.

[74] J.K.A. Clarke, M.J. Bradley, L.A.J. Garvie, A.J. Craven, T. Baird, J. Catal. 143 (1993) 122.

[75] S. Recchia, C. Dossi, N. Poli, A. Fusi, L. Sordelli, R. Psaro, J. Catal. 184 (1999) 1.

[76] L. Bednarova, C.E. Lyman, E. Rytter, A. Holmen, J. Catal. 211 (2002) 335.

[77] J. Silvestre-Albero, J.C. Serrano-Ruiz, A. Sepúlveda-Escribano, F. Rodríguez-Reinoso, Appl. Catal. A 351 (2008) 16.

[78] F. Boccuzzi, A. Chiorino, G. Ghiotti, F. Pinna, G. Strukul, R. Tessari, J. Catal. 126 (1990) 381.

[79] A.V. Kalinkin, M.Yu. Smirnov, A.I. Nizovskii, V.I. Bukhtiyarov, J. Electron. Spectrosc. Relat. Phenom. 177 (2010) 15.

[80] J.Z. Shyu, K. Otto, Appl. Surf. Sci. 32 (1988) 246.

[81] Practical Surface Analysis by Auger and X-ray photoelectron spectroscopy, Vol. 1, John Wiley & Sons, Chichester, 1990, p. 657.

[82] W.A. Coghlan, R.E. Clausing. Auger Catalog, Atomic data 5 (4) (1973) 317.

[83] Inorganic Crystal Structure Database (ICSD) reference code 105852; 105855.

[84] D.I. Kochubey, EXAFS Spectroscopy of Catalysts, Nauka, Novosibirsk, 1992, p. 145 (in Russian).

[85] S. Sakellson, M. McMillan, G.L. Haller, J. Phys. Chem. 90 (1986) 1733.

**Table captions.**

**Table 1.** Chemical composition of Mg(Zn)$AlO_x$ samples with different zinc content. Before measurements, the samples were calcined at 823 K.

**Table 2.** Microstructural characteristics of Mg(Zn)Al-$CO_3$ LDH samples.

**Table 3.** Main textural characteristics of Mg(Zn)$AlO_x$ samples according to nitrogen adsorption data. The samples were calcined at 823 K.

**Table 4.** Dispersion of supported platinum in 0.3%Pt/Mg(Zn)$AlO_x$ samples. Before measurements, the samples were calcined at 823 K and reduced in hydrogen at 823 K.

**Table 5.** Parameters of samples microstructure obtained by the simulation from experimental EXAFS spectra and parameters taken from the Structure Database [83]. *N* – partial coordination numbers, *R* – interatomic distances.

**Figure captions.**

**Fig. 1.** Micrographs of the samples: MgAl-OH (a), Mg(Zn)Al-OH-0.1 (b), ZnAl-OH (c). (Mg+Zn)/Al = 2, a X30 000 magnification.

**Fig. 2.** TEM image of sample 1%Pt/Mg(Zn)$AlO_x$-0.5 ($M^{2+}/Al^{3+}$ = 2) with atomic composition obtained from EDX-spectra of two regions.

**Fig. 3.** The adsorption-desorption isotherms (a) and pore size distribution curves (PSDC) calculated by the BJH method from the adsorption branch (b) for Mg(Zn)$AlO_x$ samples with the atomic ratio Zn/(Mg+Zn) = 0, 0.1, 0.2, 0.5, 0.7, 1.0, curves 1-6, respectively. All the samples were synthesized from Mg(Zn)Al-$CO_3$ calcined at 823 K.

**Fig. 4.** The adsorption with respect to $CO_2$ for samples $MgAlO_x$ (1), Mg(Zn)$AlO_x$-0.5 (2) and $ZnAlO_x$ (3) with the ratio (Mg+Zn)/Al = 2. Temperature of $CO_2$ adsorption was 303 K, the desorption temperature was 303, 373, 473 and 573 K.

**Fig. 5.** TPR of Mg(Zn)Al-[$PtCl_6$] calcined at 823 K. Zn/(Mg+Zn) = 0, 0.1, 0.5, 0.7, 1.0, curves 1-5, respectively. Platinum content was 0.3 wt. %.

**Fig. 6.** STEM-HAADF and TEM images of samples 1%Pt/$MgAlO_x$, Mg/Al = 2 (a) and 1%Pt/Mg(Zn)$AlO_x$-0.5 (Zn+Mg)/Al = 2 (b) and size distribution of platinum particles (according to STEM-HAADF data) for samples 1%Pt/$MgAlO_x$ (c) and 1%Pt/Mg(Zn)$AlO_x$-0.5 (d).

**Fig. 7.** Propane conversion and selectivity of propylene formation for 0.3%Pt/Mg(Zn)$AlO_x$ samples versus the fraction of Zn.

**Fig. 8.** The Pt3$d_{5/2}$ XP spectra of platinum in 1%Pt/Mg(Zn)$AlO_x$ samples with Zn/(Mg+Zn) = 0, 0.1, 0.5, 0.7; spectra 1-4, respectively. The samples were calcined at 823 K and reduced at 823 K.



Figure 1

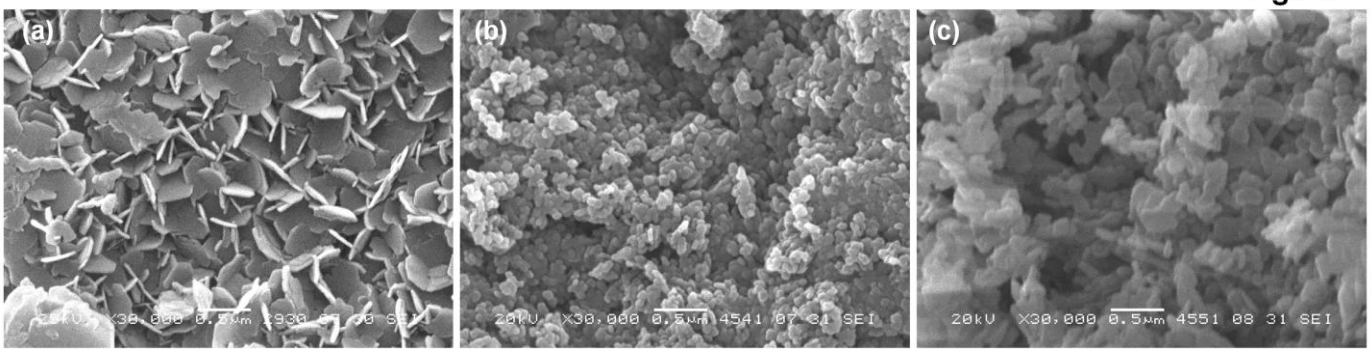

# Figure 2

| | Composition, at. % | | | (Mg+Zn)/ Al | Zn/ (Mg+Zn) |
|---|---|---|---|---|---|
| | Mg | Al | Zn | | |
| 1 | 20.5 | 20.0 | 59.5 | 4.0 | 0.7 |
| 2 | 36.9 | 31.4 | 31.7 | 2.2 | 0.5 |

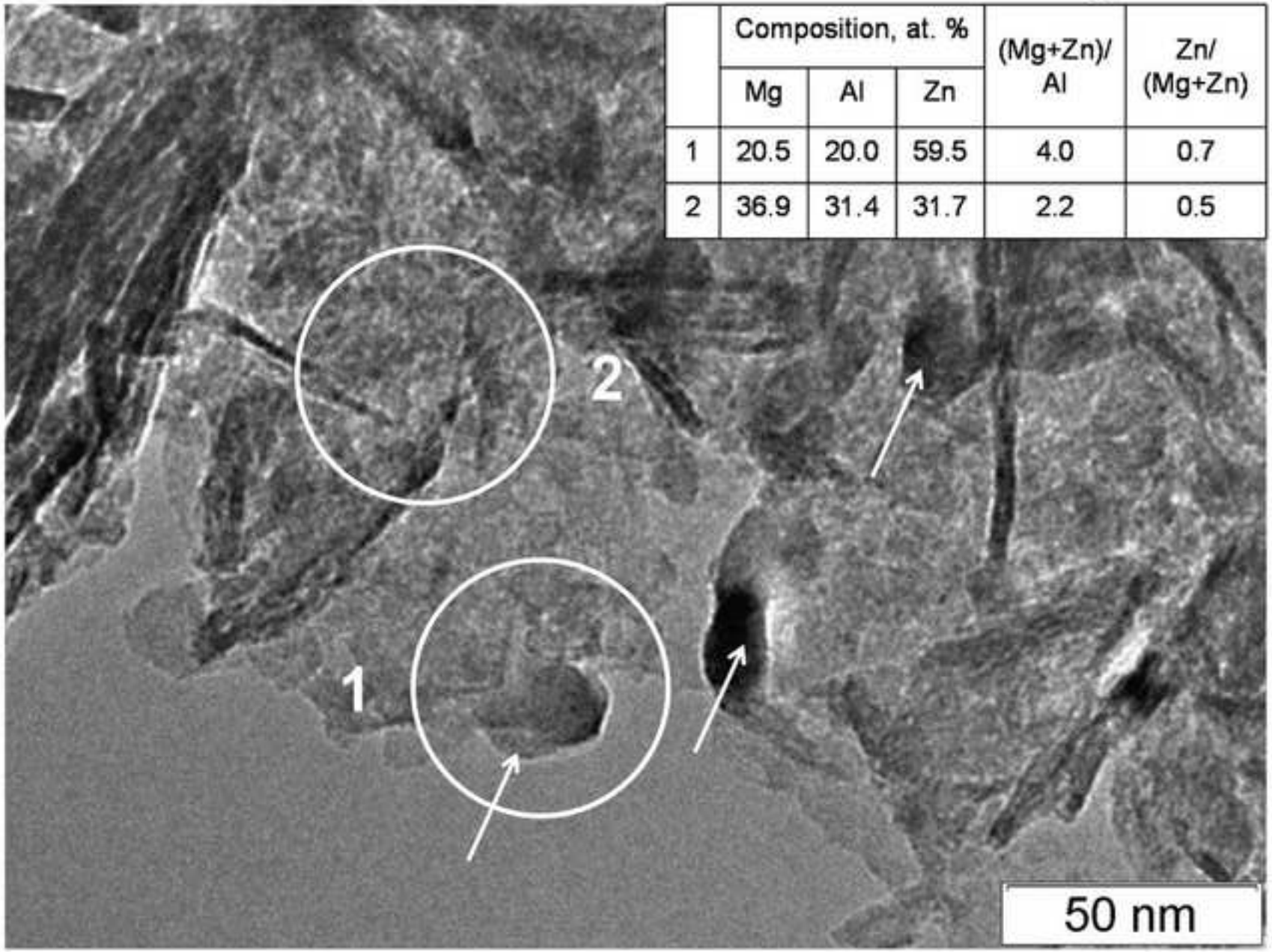

Figure 3

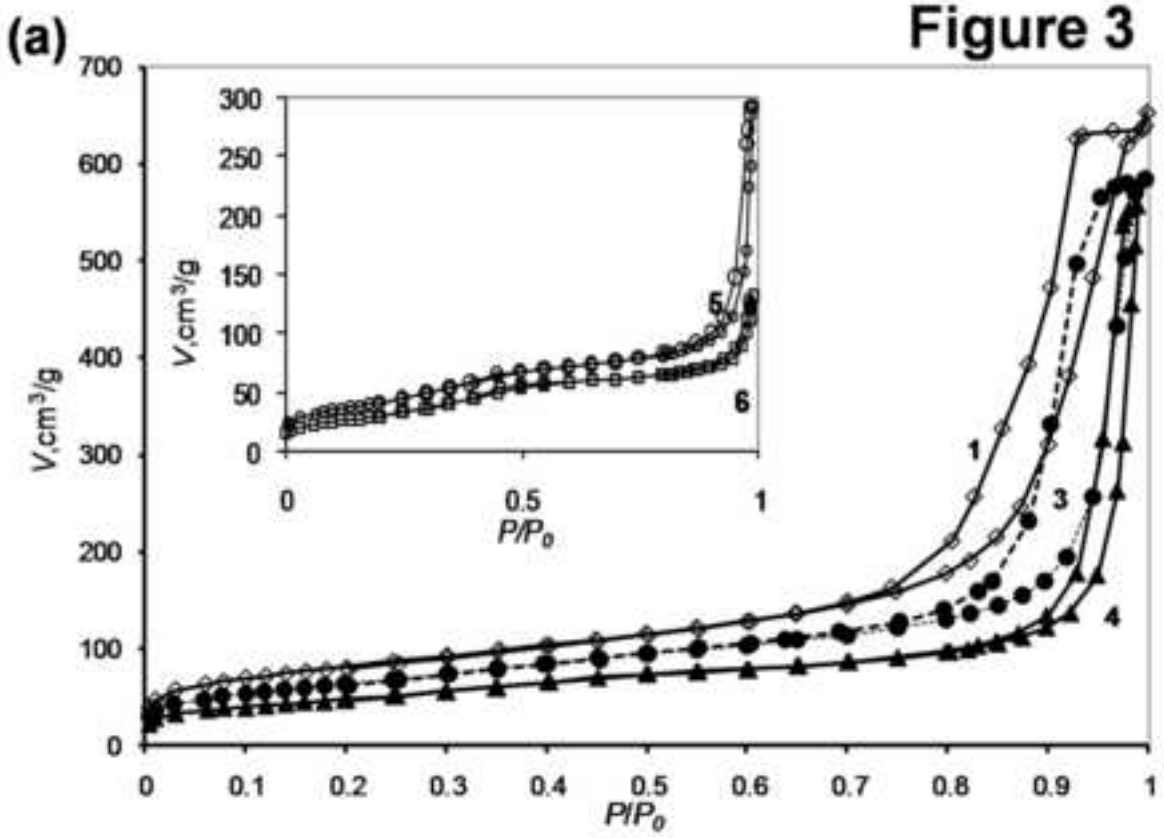


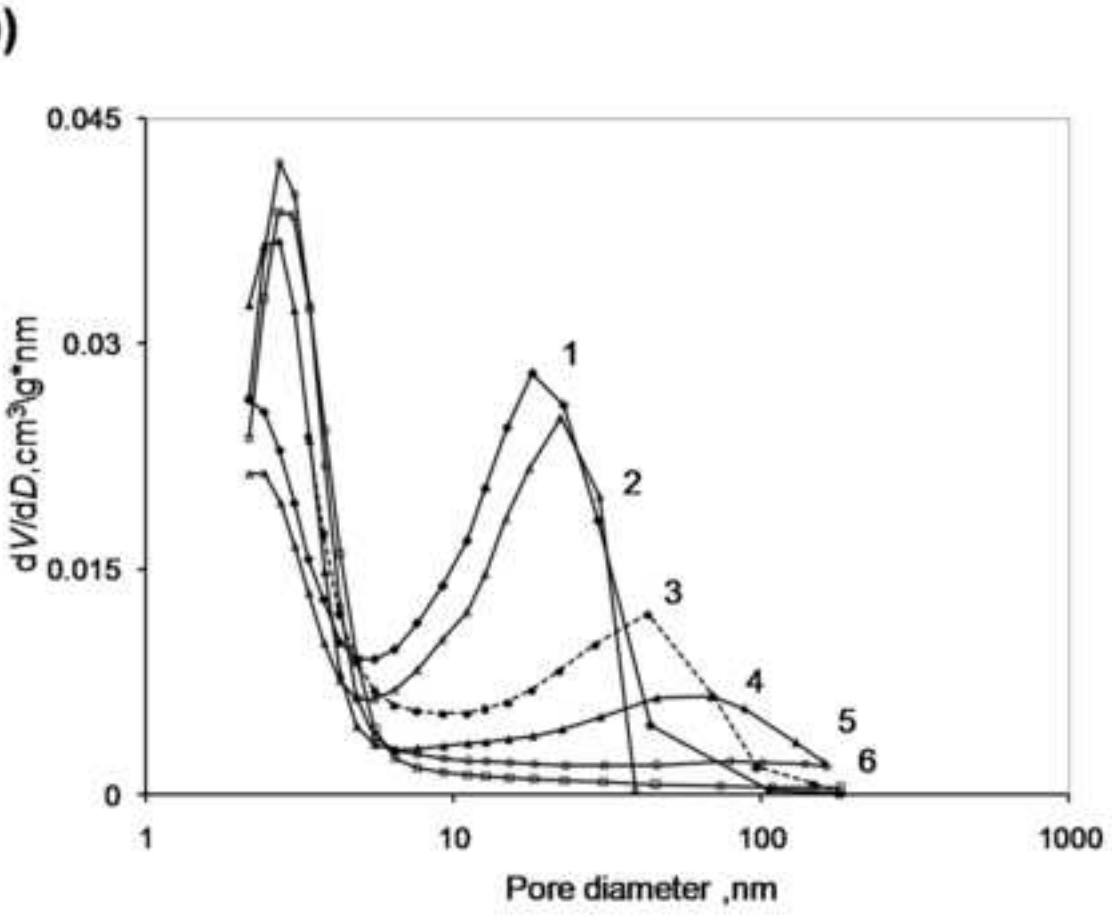

Figure



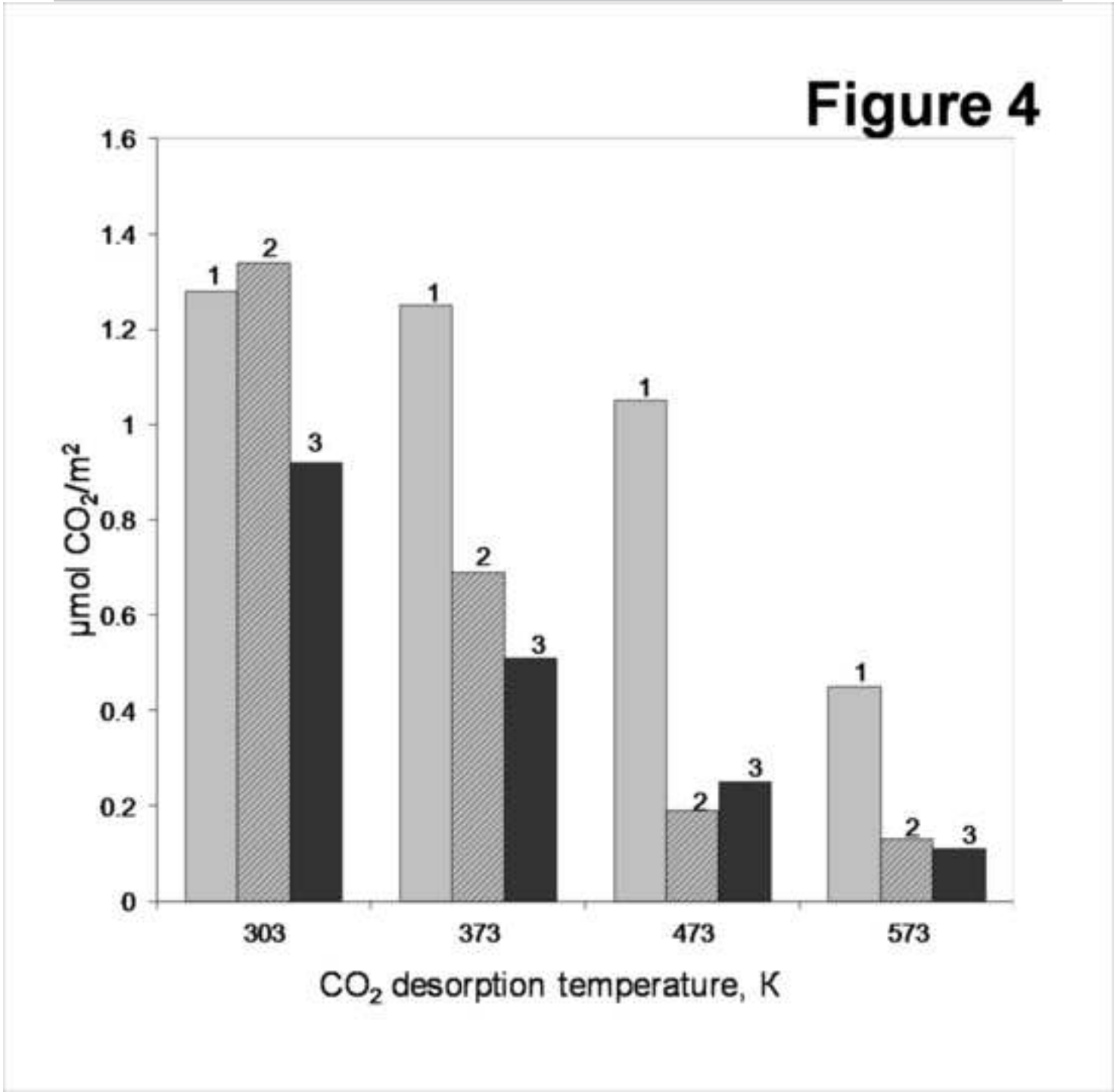

# Figure 5

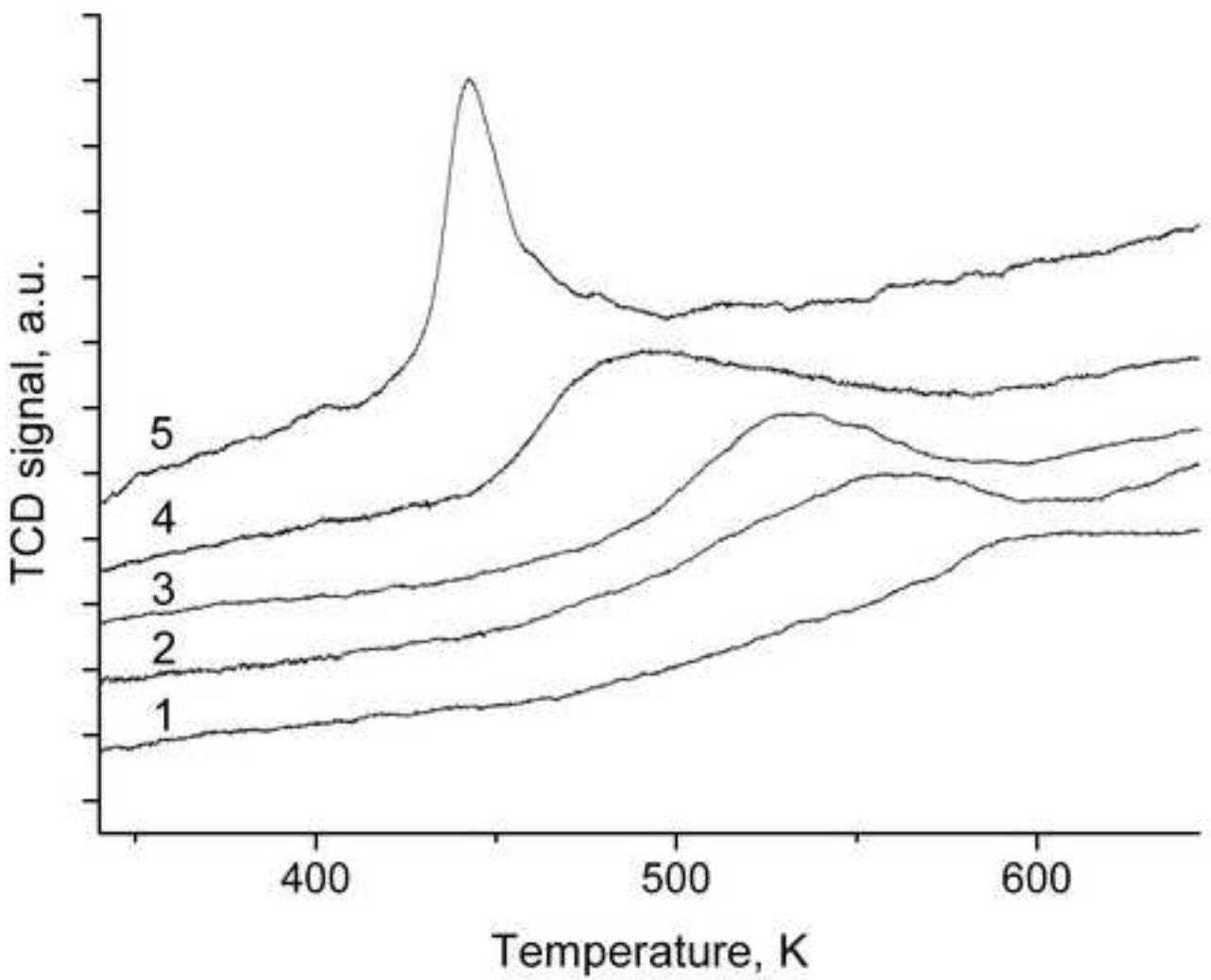

Figure 6

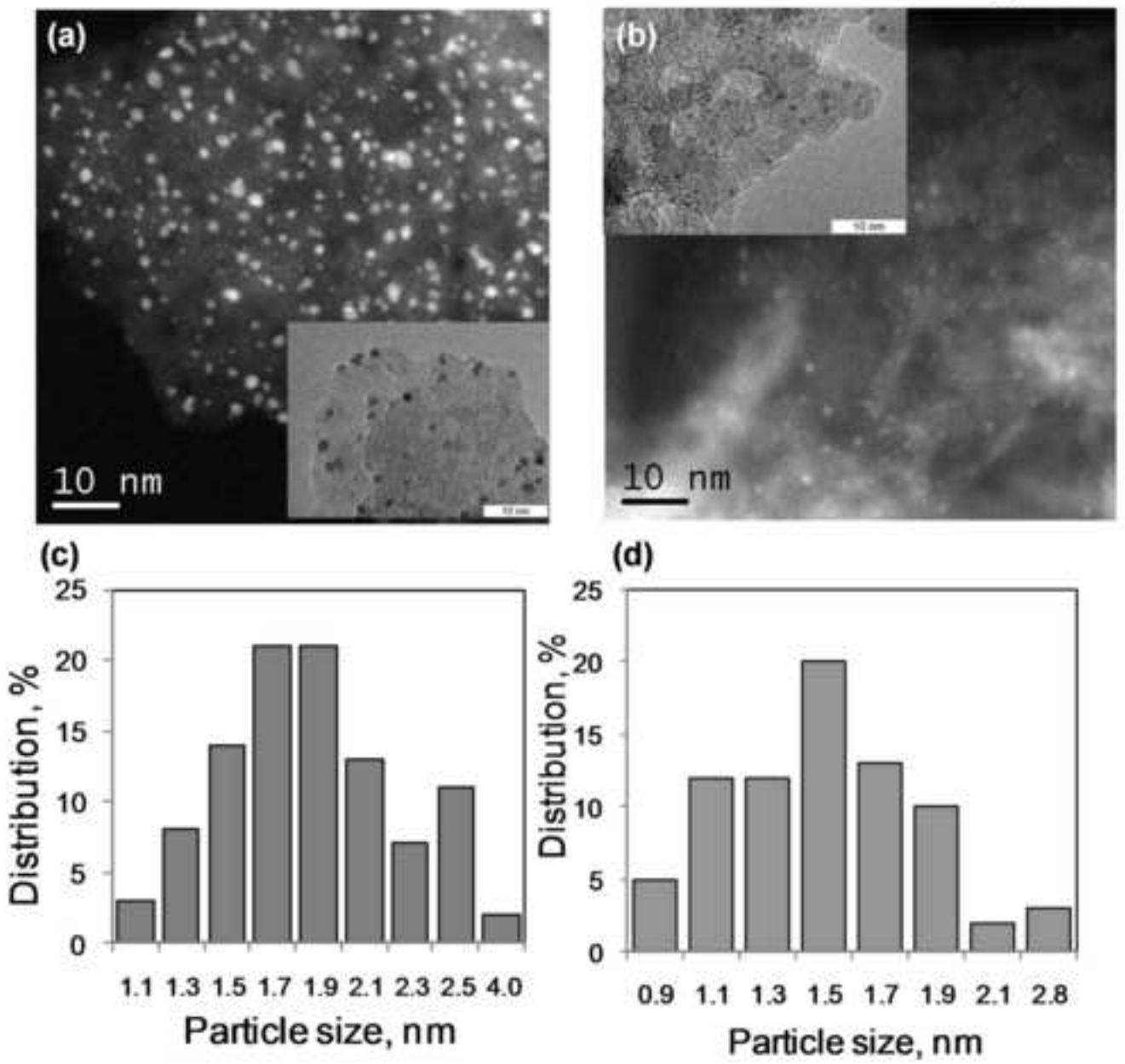

Figure 7

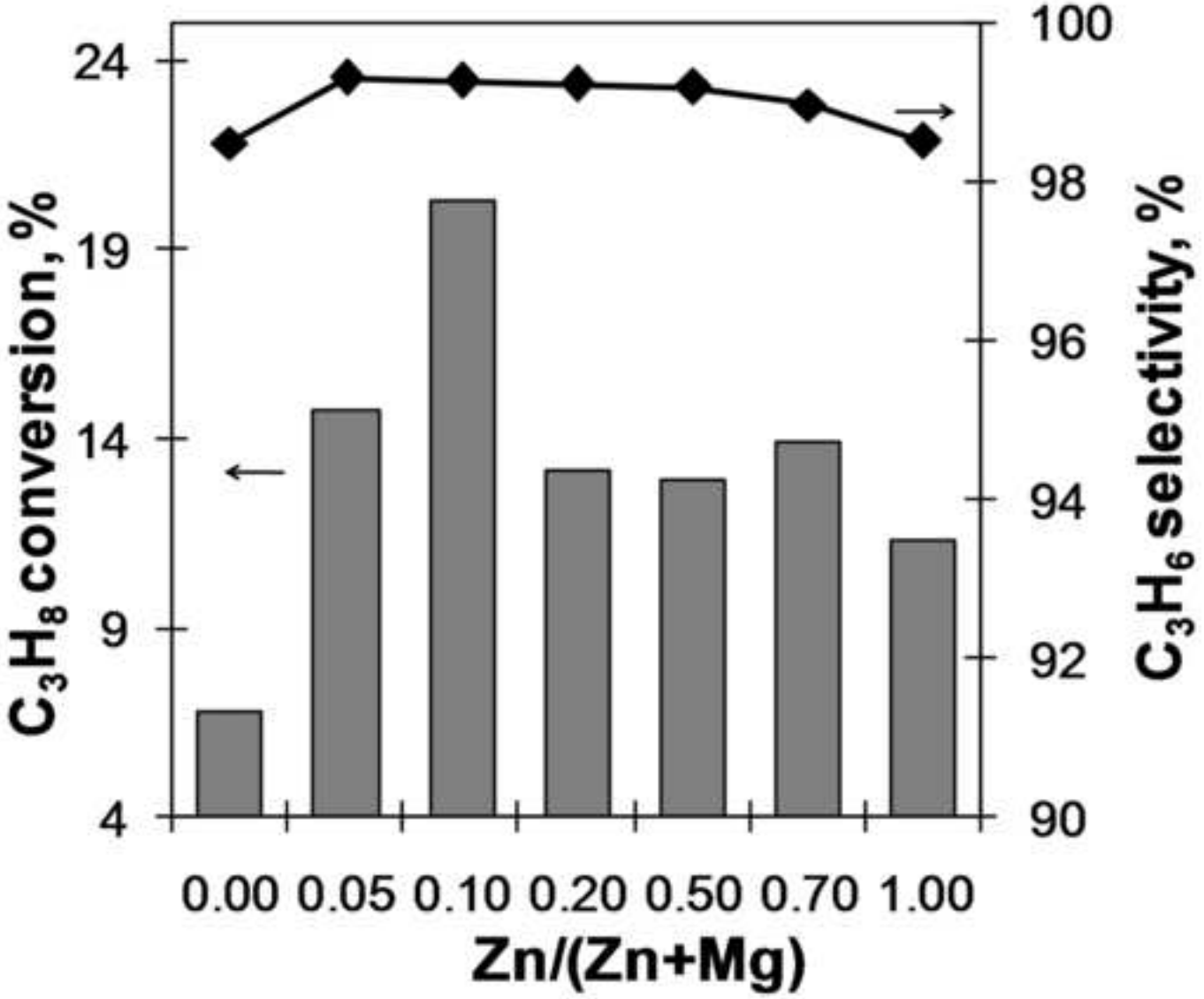

Figure 8

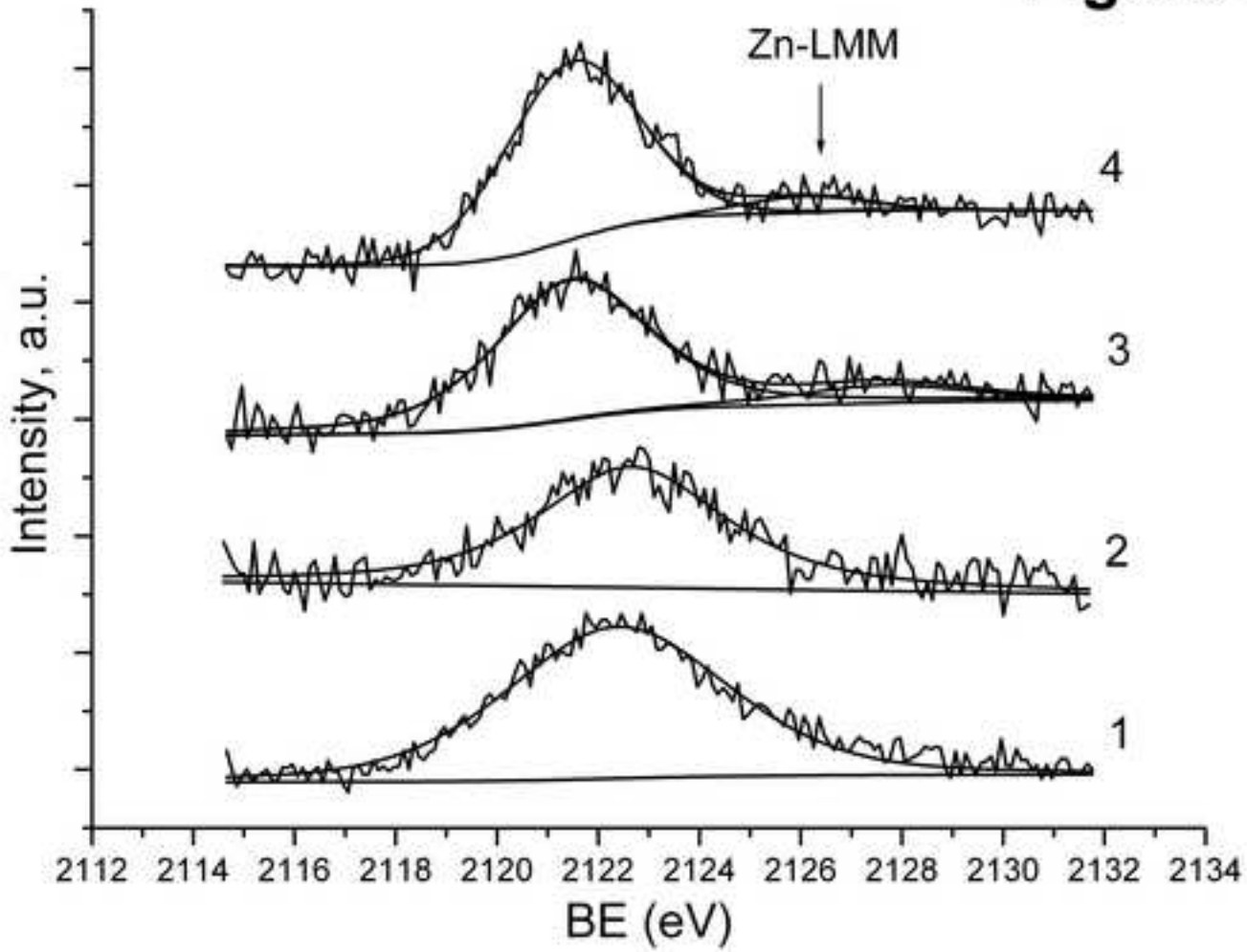

Figure 8

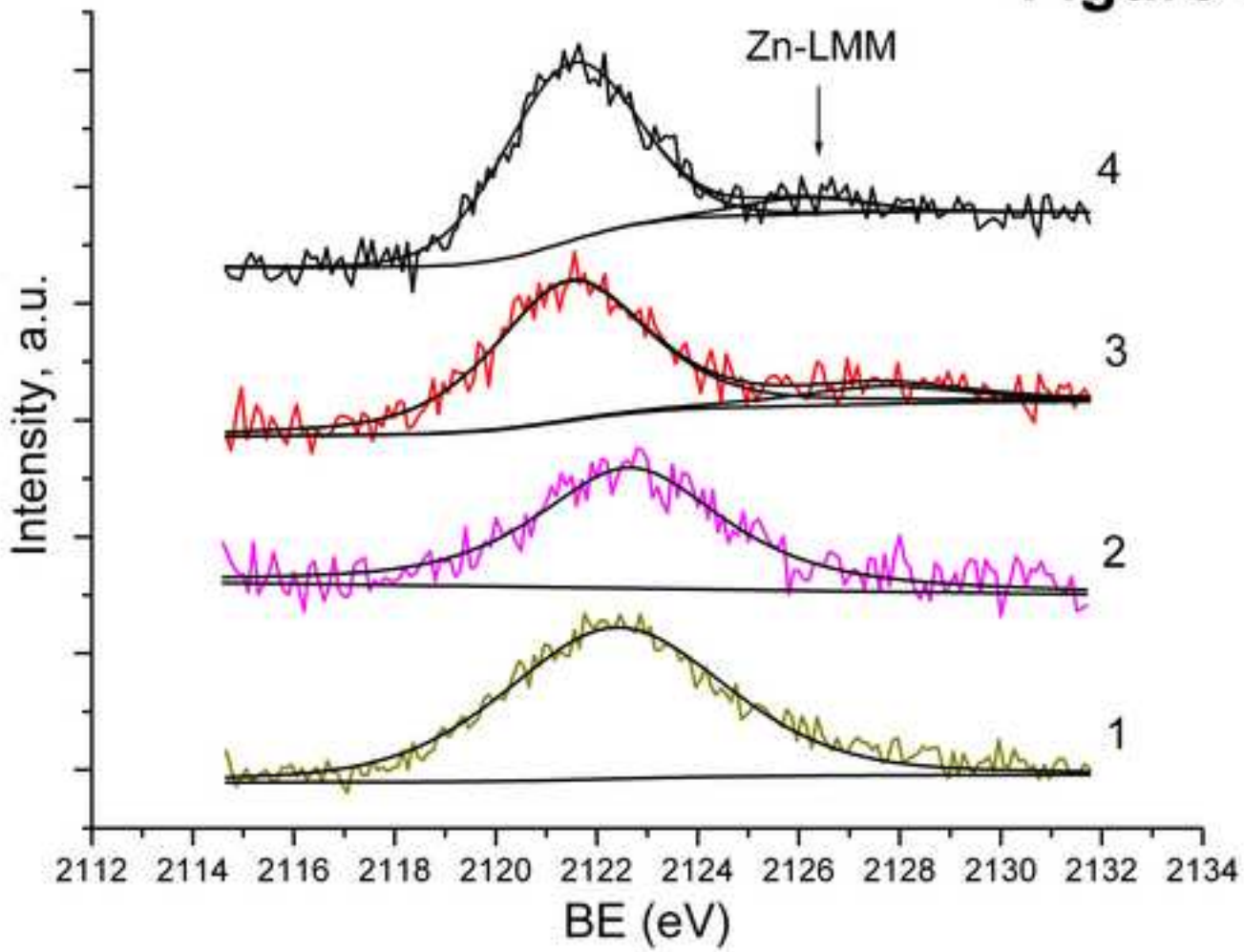

**Table 1.** Chemical composition of Mg(Zn)$AlO_x$ samples with different zinc content. Before measurements, the samples were calcined at 823 K.

| Sample | Content of elements, wt. %* | | | (Mg+Zn)/Al, at./at.* | Zn/(Zn+Mg), at./at. | | Pt/Al (XPS**) | BE Pt3$d_{5/2}$, eV** |
|---|---|---|---|---|---|---|---|---|
| | Mg | Zn | Al | | chem. analysis | XPS** | | |
| $MgAlO_x$ | 31.2 | - | 16.9 | 2.0 | 0 | - | 0.0063 | 2122.4 |
| Mg(Zn)$AlO_x$-0.05 | 30.8 | 4.7 | 14.7 | 2.4 | 0.05 | - | - | - |
| Mg(Zn)$AlO_x$-0.1 | 28.3 | 8.4 | 16.0 | 2.2 | 0.10 | 0.18 | 0.0067 | 2122.7 |
| Mg(Zn)$AlO_x$-0.2 | 22.2 | 13.6 | 13.0 | 2.3 | 0.19 | - | - | - |
| Mg(Zn)$AlO_x$-0.5 | 13.6 | 34.5 | 13.7 | 2.1 | 0.49 | 0.58 | 0.0071 | 2121.5 |
| Mg(Zn)$AlO_x$-0.7 | 7.9 | 48.1 | 12.1 | 2.4 | 0.69 | 0.63 | 0.0075 | 2121.4 |
| $ZnAlO_x$ | - | 60.9 | 10.7 | 2.3 | 1 | - | - | - |

** Results of chemical analysis of the samples by ICP OES.*
*** XPS data were obtained for 1%Pt/Mg(Zn)$AlO_x$ samples*
*Prior to XPS measurement, the samples were calcined at 823 K and reduced in hydrogen at 823 K*

**Table 2.** Microstructural characteristics of Mg(Zn)Al-$CO_3$ LDH samples.

| **Sample** | ***c*, Å** | ***a*, Å** | $L_c$, Å* | $L_a$, Å* |
|---|---|---|---|---|
| MgAl-$CO_3$ | 22.78 | 3.044 | 134 | 178 |
| Mg(Zn)Al-$CO_3$ -0.1 | 22.76 | 3.047 | 128 | 196 |
| Mg(Zn)Al-$CO_3$ -0.2 | 22.76 | 3.052 | 144 | 201 |
| Mg(Zn)Al-$CO_3$ -0.5 | 22.75 | 3.058 | 232 | 294 |
| Mg(Zn)Al-$CO_3$ -0.7 | 22.72 | 3.064 | 350 | 305 |
| ZnAl-$CO_3$ | 22.70 | 3.072 | 534 | 273 |
| Mg(Zn)Al-$PtCl_6$ -0.2 (1% Pt) | 22.84 | 3.050 | 87 | 140 |
| Mg(Zn)Al-$PtCl_6$ -0.2 (4% Pt) | 23.06 | 3.053 | 90 | 157 |

* crystallite sizes in directions *c* and *a*

**Table 3.** Main textural characteristics of Mg(Zn)$AlO_x$ samples according to nitrogen adsorption data. The samples were calcined at 823 K.

| **Sample** | $S_{BET}$, $m^2/g$ | $V_{ads,}$ $cm^3/g$ | ***D*, nm** |
|---|---|---|---|
| $MgAlO_x$ | 287 | 0.98 | 13.6 |
| Mg(Zn)$AlO_x$ - 0.1 | 250 | 0.86 | 13.8 |
| Mg(Zn)$AlO_x$ - 0.2 | 230 | 0.89 | 15.5 |
| Mg(Zn)$AlO_x$ - 0.5 | 170 | 0.86 | 20.3 |
| Mg(Zn)$AlO_x$ - 0.7 | 150 | 0.45 | 12.1 |
| $ZnAlO_x$ | 111 | 0.20 | 7.4 |

**Table 4.** Dispersion of supported platinum in 0.3%Pt/Mg(Zn)$AlO_x$ samples and TOF for the propylene formation. Before measurements, the samples were calcined at 823 K and reduced in hydrogen at 823 K.

| Sample | Pt content, wt. % | Gases uptakes n, µmol/g | | Platinum dispersion *D*(Pt), % | | TOF $mol(C_3H_8)/(mol_{Pt}\ h)$* |
|---|---|---|---|---|---|---|
| | | $H_2$ | CO | *D*($H_2$) | *D*(CO) | |
| $Pt/AlMgO_x$ | 0.35 | 2.84 | 4.59 | 32 | 26 | 257 |
| $Pt/Mg(Zn)AlO_x$-0.1 | 0.28 | 1.49 | 2.91 | 21 | 20 | 1273 |
| $Pt/Mg(Zn)AlO_x$-0.5 | 0.33 | 1.64 | 3.46 | 19 | 20 | 687 |
| $Pt/Mg(Zn)AlO_x$-0.7 | 0.35 | - | 3.41 | - | 18 | 775 |
| $Pt/AlZnO_x$ | 0.36 | 2.62 | 3.53 | 28 | 19 | 579 |

*TOF were calculated using the dispersion of platinum determined by the CO pulse chemisorption

**Table 5**. Parameters of samples microstructure obtained by the simulation from experimental EXAFS spectra and parameters taken from the Structure Database [85]. *N* – partial coordination numbers, *R* – interatomic distances.

| Sample | Absorbing atom – Backscattering atom | *N* | *R*, Å |
|---|---|---|---|
| $Pt/MgAlO_x$ | Pt – O | 2.7±0.2 | 1.97±0.01 |
| | Pt – Pt | 6.0±0.7 | 2.73±0.01 |
| $Pt/Mg(Zn)AlO_x$-0.05 | Pt – O | 2.6±0.3 | 2.04±0.01 |
| | Pt – Zn | 1.1±0.7 | 2.67±0.02 |
| | Pt – Pt | 0.8±1.2 | 2.85±0.05 |
| $Pt/Mg(Zn)AlO_x$-0.1 | Pt – O | 2.7±0.3 | 2.01±0.01 |
| | Pt – Zn | 1.8±0.7 | 2.57±0.01 |
| | Pt – Pt | 1.2±0.8 | 2.78±0.01 |
| $Pt/Mg(Zn)AlO_x$-0.5 | Pt – O | 0.5±0.2 | 1.89±0.01 |
| | Pt – Zn | 3.4 | 2.44 |
| | Pt – Zn | 3.0 ±1.0 | 2.58 ±0.02 |
| | Pt - Zn | 4.3 | 2.82 |
| $Pt/Mg(Zn)AlO_x$-0.7 | Pt – O | 0.5±0.2 | 1.90±0.01 |
| | Pt – Zn | 3.0 | 2.44 |
| | Pt – Zn | 2.7 ±1.0 | 2.59 ±0.02 |
| | Pt - Zn | 4.7 | 2.85 |
| Inorganic Crystal Structure Database [85] | | | |
| Pt metal | Pt - Pt | | 2.77 |
| $Pt_3O_4$ | Pt – O | | 1.97 |
| | Pt - Pt | | 2.79 |
| $Pt_1Zn_1$ | Pt – Zn | | 2.68 |
| | Pt - Pt | | 2.86 |
| $Pt_1Zn_{1.68}$ | Pt – Zn | | 2.57 |
| | Pt - Pt | | 2.74 |

Graphical Abstract



**Highlights**

- Zinc containing layered double hydroxides (LDH) synthesis.
- Propane dehydrogenation on the platinum catalysts based on Mg(Zn)Al-LDH .
- Electronic state of platinum in the Pt/Mg(Zn)$AlO_x$ catalysts.